Cvt9/Gsa9 Functions in Sequestering Selective Cytosolic Cargo Destined for the Vacuole

John Kim,* Yoshiaki Kamada,‡ Per E. Stromhaug,§ Ju Guan,* Ann Hefner-Gravink,* Misuzu Baba,¶ Sidney V. Scott, Yoshinori Ohsumi,‡ William A. Dunn, Jr.,‖ and Daniel J. Klionsky***

*Department of Biology, University of Michigan, Ann Arbor, Michigan 48109; ‡Department of Cell Biology, National Institute for Basic Biology, Okazaki 444-8585, Japan; §Institute for Cancer Research, Department of Cell Biology, The Norwegian Radium Hospital, Montebello, N-0310 Oslo, Norway; ‖Department of Anatomy and Cell Biology, University of Florida College of Medicine, Gainesville, Florida 32610; ¶Department of Chemical and Biological Sciences, Faculty of Science, Japan Women's University, Tokyo 112, Japan; and **Section of Microbiology, University of California at Davis, Davis, California 95616

Abstract. Three overlapping pathways mediate the transport of cytoplasmic material to the vacuole in *Saccharomyces cerevisiae*. The cytoplasm to vacuole targeting (Cvt) pathway transports the vacuolar hydrolase, aminopeptidase I (API), whereas pexophagy mediates the delivery of excess peroxisomes for degradation. Both the Cvt and pexophagy pathways are selective processes that specifically recognize their cargo. In contrast, macroautophagy nonselectively transports bulk cytosol to the vacuole for recycling. Most of the import machinery characterized thus far is required for all three modes of transport. However, unique features of each pathway dictate the requirement for additional components that differentiate these pathways from one another, including at the step of specific cargo selection.

We have identified Cvt9 and its *Pichia pastoris* counterpart Gsa9. In *S. cerevisiae*, Cvt9 is required for the selective delivery of precursor API (prAPI) to the vacuole by the Cvt pathway and the targeted degradation of peroxisomes by pexophagy. In *P. pastoris*, Gsa9 is required for glucose-induced pexophagy. Significantly, neither Cvt9 nor Gsa9 is required for starvation-induced nonselective transport of bulk cytoplasmic cargo by macroautophagy. The deletion of *CVT9* destabilizes the binding of prAPI to the membrane and analysis of a *cvt9* temperature-sensitive mutant supports a direct role of Cvt9 in transport vesicle formation. Cvt9 oligomers peripherally associate with a novel, perivacuolar membrane compartment and interact with Apg1, a Ser/Thr kinase essential for both the Cvt pathway and autophagy. In *P. pastoris* Gsa9 is recruited to concentrated regions on the vacuole membrane that contact peroxisomes in the process of being engulfed by pexophagy. These biochemical and morphological results demonstrate that Cvt9 and the *P. pastoris* homologue Gsa9 may function at the step of selective cargo sequestration.

Key words: autophagy • degradation • lysosome • peroxisome • vacuole

Introduction

General cell function and homeostasis require the regulated counterbalancing of protein synthesis and organelle biogenesis with protein breakdown and the selective degradation of organelles. The macroautophagy pathway directs the lysosome-mediated breakdown of bulk cytoplasm, including proteins, nucleic acids, lipids, and organelles and serves as the principal cellular degradative process (for review see Klionsky and Ohsumi, 1999; Kim and Klionsky, 2000). The general mechanism of autophagy has been conserved from yeast to mammals. In yeast, starvation conditions mobilize the autophagic machinery to deliver cytoplasmic constituents to the vacuole, where substrate digestion and recycling mechanisms ensure cell survival. In mammals, macroautophagy has also been implicated to play a role in cellular remodeling during development, differentiation, and aging (Mortimore et al., 1996; Vittorini et al., 1999). In addition, recent findings that a dysfunctional autophagy pathway may contribute to the metastasis of certain types of cancers further underscore the relevance of autophagic degradation processes in humans (Liang et al., 1999; for review see Klionsky and Emr, 2000).

Biochemical and microscopy studies have outlined the basic steps of macroautophagy in *Saccharomyces cerevisiae* (for review see Klionsky and Ohsumi, 1999). Upon induction, double-membrane vesicles, termed autophagosomes, capture bulk cytoplasm before being targeted to the vacuole.

Address correspondence to Daniel J. Klionsky, Department of Biology, University of Michigan, Ann Arbor, MI 48109. Tel.: (734) 615-6556. Fax: (734) 647-0884. E-mail: klionsky@umich.edu

Fusion of the autophagosome with the vacuole membrane releases a single-membrane vesicle, the autophagic body, into the vacuolar lumen. Subsequent breakdown of the autophagic body releases its cytoplasmic contents for digestion and recycling.

Insights into the molecular details of macroautophagy have been greatly facilitated through molecular genetic studies in *S. cerevisiae* (Tsukada and Ohsumi, 1993; Thumm et al., 1994; for review see Kim and Klionsky, 2000). The cloning of the genes that complement these yeast macroautophagy mutants, *apg* and *aut*, has subsequently led to the identification of mammalian homologues of key macroautophagy components, thus supporting the conserved nature of this pathway across eukaryotic kingdoms. The identified machinery includes a group of components required for transducing the signal for autophagy induction to downstream effectors. Chief among these is the phosphatidylinositol 3-kinase homologue, Tor. Activation of Tor represses autophagy, whereas its inhibition by nutrient starvation conditions or with the immunosuppressant drug rapamycin triggers the pathway (Noda and Ohsumi, 1998). The activity of Tor also affects the phosphorylation state of Apg13 and the downstream kinase activity of Apg1 (Kamada et al., 2000). Tor-dependent hyperphosphorylation of Apg13 lessens the affinity of Apg13 for the Apg1 kinase and results in reduced kinase activity as well as the inhibition of autophagy. Conversely, Tor repression leads to decreased phosphorylation of Apg13, an increase in the interaction between Apg13 and Apg1, and the induction of autophagy.

The formation and completion of autophagosomes requires the function of a novel Apg protein conjugation system which results in the covalent linkage of Apg12 to Apg5 (Kametaka et al., 1996; Mizushima et al., 1998; George et al., 2000). The intermediate steps leading to Apg12–Apg5 conjugation involve Apg7, an E1 ubiquitin activating enzyme homologue, and Apg10, which functions as a protein conjugating enzyme (Mizushima et al., 1998; Kim et al., 1999; Shintani et al., 1999; Tanida et al., 1999). After conjugation of Apg12 to Apg5, the Apg16 protein binds Apg5 noncovalently and dimerizes to link a pair of conjugates (Mizushima et al., 1999). Mutations in any one of these components result in the failure of autophagic vesicle formation/completion. Once completed, autophagosome docking and fusion with the vacuole requires predicted vesicle fusion machinery, including the homologues of syntaxin (Vam3; Darsow et al., 1997), SNAP-25 (Vam7; Sato et al., 1998), and a rab-GTPase (Ypt7; Kim et al., 1999), as well as the class C Vps protein complex (Rieder and Emr, 1997; Scott et al., 1997; Sato et al., 2000; Seals et al., 2000). Successful fusion of the autophagosome with the vacuole membrane releases the single-membrane autophagic body into the vacuole lumen (Takeshige et al., 1992; Baba et al., 1994, 1995). Breakdown of these vesicles, which exposes the autophagic cargo for digestion and recycling, requires the acidification of the vacuole (Nakamura et al., 1997), as well as the vacuolar protease Prb1 (Takeshige et al., 1992) and the putative lipase Cvt17 (Scott et al., 1997; Teter et al., 2001).

The majority of the components required for starvation-induced macroautophagy are also employed to transport selective cargo. Under nutrient-rich conditions, the cytoplasm to vacuole targeting (Cvt)[1] pathway transports the resident hydrolase aminopeptidase I (API) to the vacuole (Klionsky et al., 1992). The overlap in transport machinery between autophagy and the Cvt pathway reflects the mechanistic similarities between the two pathways (Harding et al., 1996; Scott et al., 1996). Precursor API (prAPI) is packaged in double-membrane vesicles (Cvt vesicles) that are substantially smaller than autophagosomes and appear to exclude bulk cytoplasm (Baba et al., 1997; Scott et al., 1997). Completed Cvt vesicles fuse with the vacuole and release a single-membrane vesicle (Cvt body) into the vacuolar lumen (Scott et al., 1997). The breakdown of the Cvt body releases prAPI into its resident lumenal environment, where it is proteolytically processed to the mature form (Klionsky et al., 1992).

In addition to the Cvt pathway, macroautophagy machinery is essential for the selective delivery of excess peroxisomes to the vacuole by the related pexophagy pathway (for review see Kim et al., 2000). Defects in autophagy components compromise peroxisome degradation in *S. cerevisiae* (Hutchins et al., 1999). In the methylotrophic yeast *Pichia pastoris*, vacuole-mediated degradation of peroxisomes after glucose adaptation utilizes a micropexophagic mechanism in which designated excess peroxisomes are directly engulfed by the vacuole (Tuttle and Dunn, 1995; Sakai et al., 1998). Despite the difference in the site of sequestration, micropexophagy also clearly requires autophagic machinery as an increasing number of *P. pastoris* homologues of autophagy components are being identified (Yuan et al., 1999).

A key question that remains to be answered is what differentiates nonselelective bulk cargo from the specifically targeted cargo, such as prAPI and peroxisomes? Indiscriminate packaging of physiologically critical organelles would result in severe cellular dysfunction. On the other hand, maintaining excess organelles would be energetically wasteful, whereas the failure to sequester and degrade nonfunctional or malfunctioning organelles could result in cell death. To provide such specificity, additional factors are likely required to mediate the sequestration of particular cargo.

In this study, we have identified Cvt9 in *S. cerevisiae* and Gsa9 in *P. pastoris*, which are structural and functional homologues. Cvt9 was identified by its requirement for vacuole uptake of prAPI, and Gsa9 by its role in the turnover of peroxisomal enzymes. Although both Cvt9 and Gsa9 are required for the selective uptake of peroxisomes into the yeast vacuole for degradation, neither protein is essential for nonselective macroautophagy induced by nitrogen starvation. These proteins are associated with a unique membrane compartment located in a perivacuolar region of the cell. Our biochemical and morphological results suggest that Cvt9 and Gsa9 function to selectively sequester cytoplasmic proteins and organelles for degradation within the vacuole.

[1]*Abbreviations used in this paper:* ALP, alkaline phosphatase; AOX, alcohol oxidase; API, aminopeptidase I; BFP, blue fluorescent protein; Cvt, cytoplasm to vacuole targeting; GFP, green fluorescent protein; HA, hemagglutinin; PGK, phosphoglycerate kinase; prAPI, precursor API; SMD, synthetic minimal medium; td, temperature degron; YNB, yeast nitrogen base.

Table I. Strains Used in This Study

Name	Genotype	Reference
S. cerevisiae strains		
KA311A	*MAT*a *his3 leu2 trp1 ura3*	Irie et al., 1993
YYK36	KA311A *apg1Δ::LEU2*	This study
YYK107	KA311A *cvt9Δ::URA3*	This study
SEY6210	*MATα ura3-52 leu2-3,112 his3-Δ200 trp1-Δ901 lys2-801 suc2-Δ9 mel GAL*	Robinson et al., 1988
VDY101	SEY6210 *apg7Δ::LEU2*	Kim et al., 1999
JKY007	SEY6210 *apg9Δ::HIS3*	Noda et al., 2000
THY119	SEY6210 *cvt3-1*	Harding et al., 1995
AHY001	SEY6210 *cvt9Δ::HIS3*	This study
AHY96	SEY6210 *cvt9-1*	Harding et al., 1996
JGYtd9	SEY6210 *cvt9Δ::CVT9*-DHFR-Ub-HA	This study
AHY1468	SEY6210 *cvt10-1*	Harding et al., 1996
TVY1	SEY6210 *pep4Δ::LEU2*	Gerhardt et al., 1998
WSY99	SEY6210 *ypt7Δ::HIS3*	Wurmser and Emr, 1998
TN121	*MATa leu2-3,112 trp1 ura3-52 pho8Δ::pho8Δ60 pho13Δ::URA3*	Noda et al., 1995
AHY021	TN121 *cvt9Δ::LEU2*	This study
TN125	*MAT*a *ade2 his3 leu2 lys2 trp1 ura3 pho8::pho8Δ60*	Noda and Ohsumi, 1998
YYK126	TN125 *apg1Δ::LEU2*	Kamada et al., 2000
YYK127	TN125 *cvt9Δ::LEU2*	This study
P. pastoris strains		
GS115	*his4*	Cregg et al., 1985
WDY7	*his4 gsa7*	Yuan et al., 1999
R8	GS115 *gsa9-2*::Zeocin	This study
WDY26	GS115 *his4*::pWD11 (P_{GAP} HA-GSA9, HIS4)	This study
DMM1	GS115::pDM1 (P_{AOX1}GFP-SKL, Zeocin)	This study
ANB23	DMM1 *his4*::pPS64 (P_{GAP} GFP-HA-GSA9, HIS4)	This study
SMD1163	*his4 pep4 prb1*	Tuttle and Dunn, 1995
PPF1	*his4 arg4*	Yuan et al., 1997
WDK09	*PPF1 gsa9Δ::ARG4*	This study
ANB12	WDK09 *his4*::pPS64 (P_{GAP}GFP-HA-GSA9, HIS4)	This study

Materials and Methods

Strains

The yeast strains used in this study are listed in Table I.

Growth Media

S. cerevisiae strains were grown in synthetic minimal medium (SMD: 0.67% yeast nitrogen base [YNB], 2% glucose, and auxotrophic amino acids and vitamins as needed). Starvation experiments were carried out in SD-N (0.17% YNB without ammonium sulfate or amino acids, and 2% glucose). Peroxisomes were induced by growth in oleic acid medium (YTO: 0.67% YNB, 0.1% Tween 40, and 0.1% oleic acid). *P. pastoris* strains were grown in YPD (1% Bacto yeast extract, 2% Bacto peptone, and 2% glucose). Peroxisomes were induced by growth in methanol (YNM: 0.67% YNB, 0.4 mg/liter biotin, and 0.5% vol/vol methanol). Degradation of peroxisomes was carried out in YND (0.67% YNB, 0.4 mg/liter biotin, and 2% glucose).

Antibodies/Antiserum

Rabbit antisera against Cvt9 peptides corresponding to amino acids 356–382 and 534–547 (Multiple Peptide Systems) were generated as described previously (Klionsky et al., 1992). Antibodies to API, Fox3, and Apg9 have been described (Klionsky et al., 1992; Hutchins et al., 1999; Noda et al., 2000). Antiserum against phosphoglycerate kinase (PGK) and Pep12 were provided by Dr. Jeremy Thorner (University of California at Berkeley, Berkeley, CA; Baum et al., 1978) and Dr. Scott Emr (University of California at San Diego, La Jolla, CA; Becherer et al., 1996), respectively. Mouse monoclonal antibodies to Dpm1 and Pho8 were from Molecular Probes. Antisera and antibodies to the hemagglutinin (HA) and myc epitopes were from Covance Research Products, Inc.

Materials

Reagents are identical to those described previously (Kim et al., 1999; Noda et al., 2000). The copper-inducible promoter-based vectors, pCu416, pCu414, and pCu426, were gifts from Dr. Dennis J. Thiele (University of Michigan, Ann Arbor, MI; Labbé and Thiele, 1999). The pREMI vector was a gift from Dr. Benjamin S. Glick (University of Chicago, Chicago, IL). The pGFP(416)SK and pGFP(426)SK vectors for expressing green fluorescent protein (GFP) fusions were a gift from Dr. Tom Vida (University of Texas Health Sciences Center, Houston, TX). The temperature degron (td) plasmid was a gift from Dr. Jürgen Dohmen (University of Cologne, Cologne, Germany; Dohmen et al., 1994).

Cloning CVT9

The *cvt9* strain AHY96 (Harding et al., 1996) was transformed with a YCp50-based yeast genomic library (Rose et al., 1987). The transformed colonies were subjected to a nitrogen starvation screen as described previously (Kim et al., 1999). After 30 d, 1 colony out of the first 100 survivors examined contained mature API. The complementing plasmid was recovered and sequenced using pBR322 oligonucleotides. Partial sequences were entered into the *Saccharomyces* genome database (SGD; http://genome-www.stanford.edu/Saccharomyces/) and a 20.9-kb region on chromosome XVI was identified. A 4,812-bp fragment that complemented the prAPI maturation defect was introduced into pRS414 and pRS424 by using the endogenous SpeI-BamHI restrictions sites, resulting in the pCVT9(414) and pCVT9(424) clones. These clones contain the 3,537-bp *CVT9* ORF (YPR049C) plus 585 bp of the 5′ and 690 bp of the 3′ noncoding sequences. Alternatively, the *CVT9* gene was amplified from genomic DNA by PCR and cloned into the vector pBluescript to generate pBS(CVT9). A 4.8-kb SpeI-BamHI fragment containing the *CVT9* gene from pBS(CVT9) was cloned into pRS313 to generate p313(CVT9).

Isolation of gsa9 Mutants and Cloning GSA9

P. pastoris gsa mutants were isolated after the restriction enzyme–mediated integration of a 2.0-kb pREMI plasmid which contained the Col E1 origin of replication and the Zeocin resistance gene under the control of the *TEF1* promoter from *S. cerevisiae* and the EM7 promoter of *Escherichia coli*. Details of the mutagenesis procedure will be described elsewhere. Three different *gsa* mutants had a disruption of the *GSA9* gene.

gsa9-1 cells had the pREMI vector inserted between Q1068 and Y1069, *gsa9-2* between M83 and S84, and *gsa9-3* between R1291 and A1292. Using the different genomic DNA fragments from the three different allelic mutants, we were able to completely assemble the *GSA9* gene as well as 700 bp of the 5′ and 600 bp of the 3′ noncoding regions. The genomic sequence of *GSA9* reported in this paper has been deposited in the National Center for Biotechnology Information (EMBL/GenBank/DDBJ accession number AF309870).

Disruption of CVT9 and GSA9

The chromosomal *CVT9* locus was deleted by a PCR-based, one-step procedure (Noda et al., 2000). The auxotrophic *HIS3* gene was amplified from the pRS313 vector using oligonucleotides that contained vector sequences outside of the *HIS3* marker flanked by *CVT9* sequences that encode regions at the beginning and end of the *CVT9* ORF. The PCR product was used to transform yeast strain SEY6210 and the His^+ transformants were screened for prAPI accumulation to identify *CVT9* knockouts. The *cvt9*Δ strain was confirmed by tetrad analysis as described previously (Kim et al., 1999). Alternatively, a 1.1-kb BglII-EcoRV fragment from within the *CVT9* gene in the plasmid pUC19 was replaced with the *LEU2* gene. This plasmid was digested with HindIII and transformed into the TN125 yeast strain to make strain YYK127. Transformants were selected on the appropriate auxotrophic plates and screened by immunoblot using antiserum to API.

To disrupt *GSA9*, the *S. cerevisiae ARG4* gene with its promoter was amplified by PCR using primers that contained 52 bp of 5′ and 3′ regions of *GSA9* and 27 bp of the *ARG4* gene. The PCR product was directly used to transform PPF1 cells. The resulting Arg^+ clones were replica-plated to YNM plates and their inability to degrade alcohol oxidase (AOX) during glucose adaptation was determined by direct colony assay as described below. The site of *ARG4* insertion within WDK09 resulting in the deletion of >90% of the *GSA9* gene was verified by PCR.

Plasmid Constructions

Generation of Epitope-tagged Cvt9. To epitope-tag Cvt9, the BamHI site in p313(CVT9) was destroyed. A new BamHI site was created after the *CVT9* start codon by PCR to make p313[BHI-CVT9]. A DNA fragment encoding a 3×HA or 3×myc epitope with BamHI sites on both sides was then ligated into the newly created BamHI site to generate the p313[3×HA-CVT9] or p313[3×myc-CVT9] plasmid. Both plasmids complemented the prAPI accumulation phenotype of the *cvt9*Δ strain (data not shown).

The CVT9td Construct. The method of Dohmen et al. (1994) was used to construct a temperature-sensitive *cvt9* mutant. A 751-bp segment of *CVT9* was amplified by PCR using a primer that included a portion of the 5′ untranslated region and incorporated a HindIII site, and a 3′ primer that incorporated an EcoRI site. The PCR product was digested with HindIII and EcoRI. Plasmid pPW66R was digested with NotI and HindIII and the 1.4-kb fragment containing Ub-DHFRts-HA under the *CUP1* promoter was isolated. The HindIII-EcoRI fragment of *CVT9* and the NotI-HindIII fragment from pPW66R were cloned into the pRS306 vector that had been digested with NotI and EcoRI. The resulting plasmid, pCVT9td, was digested with BglII and transformed into yeast. Ura^+ transformants were screened by growing cells in the presence of copper and carrying out immunoprecipitations with antiserum to Cvt9. Strain JGYtd9 showed a copper-dependent increase in Cvt9 protein levels and was used for subsequent analyses.

Constructs of CVT9 and GFPCVT9 under CUP1 Promoter Control. The *CVT9* ORF was PCR-amplified from pCVT9(414) using oligonucleotides that incorporated an in-frame XmaI site directly upstream of the start codon on the 5′ primer and a SalI site after the stop codon on the 3′ primer. The PCR product was digested with XmaI-SalI and subcloned into pCu416, resulting in pCuCVT9(416). The same restriction-digested PCR product was subcloned into pCuGFP(416), resulting in pCuGFPCVT9(416), which contains the *CUP1*-controlled *GFP* fused to the 5′ of the *CVT9* ORF.

Gsa9 was tagged with the HA epitope at the NH_2 terminus by PCR amplification from genomic DNA. *HA-GSA9* was inserted into the KpnI and XhoI sites of pIB2 (Sears et al., 1998). This plasmid, pWD11, was linearized by cutting within the *HIS4* gene and used to transform GS115 cells. *HA-GSA9* was also inserted into the KpnI and XhoI sites behind the GFP gene, which had been inserted into the EcoRI site of pIB2. The resulting plasmid pPS64 containing GFP/*HA-GSA9* behind the constitutive and glucose-inducible GAPDH promoter was linearized by cutting within the *HIS4* gene and used to transform WDK09 and DMM1 cells.

Two-Hybrid Analysis

A two-hybrid screen was carried out using a truncated form of the *APG1* ORF lacking the NH_2-terminal eight amino acids as the bait plasmid as described (Kamada et al., 2000).

Nitrogen Survival Assay

Nitrogen starvation analysis was done as described previously (Scott et al., 1996).

Alkaline Phosphatase Enzyme Assay

Induction of autophagy was estimated as activity of mutated alkaline phosphatase (ALP; Pho8Δ60p) with α-napthyl phosphate (Sigma-Aldrich) as substrate as described (Noda and Ohsumi, 1998).

Measurements of Protein and Peroxisome Degradation

The degradation of peroxisomes in *S. cerevisiae* was determined by the loss of thiolase (Fox3) as described previously (Hutchins et al., 1999). The degradation of peroxisomes in *P. pastoris* was evaluated by measuring the loss of AOX during glucose adaptation. Samples were assayed for AOX activity as described previously (Yuan et al., 1999) at 0 and 6 h after shifting to glucose. The degradation of cellular proteins during nitrogen starvation was performed as described previously (Yuan et al., 1999).

Cell Labeling, Immunoprecipitations, and Immunoblot Analysis

Radioisotopic labeling of cells, immunoprecipitations, and immunoblotting were performed as described previously (Noda et al., 2000).

Protease Protection and Membrane Flotation Assays

Protease sensitivity of prAPI in the *cvt9td* and *ypt7*Δ strains and membrane flotation experiments were performed as described previously (Noda et al., 2000).

Subcellular Fractionations

For subcellular fractionation experiments, *cvt9*Δ cells transformed with the pCuCVT9(416) plasmid were induced with 50 μM $CuSO_4$ for 1 h at midlog stage and then spheroplasted as described previously (Kim et al., 1999). Spheroplasts were subjected to differential lysis in PS200 lysis buffer A (20 mM PIPES, pH 6.8, 200 mM sorbitol, 5 mM $MgCl_2$) containing the Complete™ EDTA-free protease inhibitor cocktail (Roche Molecular Biochemicals) and 1 mM PMSF. After a preclearing step at 100 *g*, 4°C, 5 min, the lysate was subjected to low-speed centrifugation at 16,000 *g* (13,000 rpm) in an Eppendorf 5415D microcentrifuge for 5 min at 4°C. The low-speed supernatant fraction (S13) was further resolved into high-speed supernatant and pellet fractions (S100 and P100, respectively) by centrifugation at 100,000 *g* for 20 min at 4°C in a centrifuge (TL100) using a TLA100.4 rotor (both from Beckman Coulter).

For the biochemical characterization of Cvt9 membrane association, the total lysate was mixed with an equal volume of 1% Triton X-100 (in PS200), 6 M urea (in PS200), 0.1 M Na_2CO_3, pH 10.5 (in 200 mM sorbitol), or a 1.0 M salt wash (0.67 M KOAc, 0.3 M KCl). After a 5-min incubation at 25°C, the treated lysates were separated into high speed supernatant and pellet fractions by centrifugation at 100,000 *g* for 20 min at 4°C.

To assess prAPI binding, *cvt9*Δ spheroplasts were lysed in PS200 containing 0, 1, 2, or 5 mM $MgCl_2$ and separated into low-speed supernatant and pellet fractions by centrifugation at 2,300 *g* (5,000 rpm) in an Eppendorf 5415D microcentrifuge for 5 min at 25°C. All fractionated samples were subjected to immunoblot analysis.

Optiprep Gradient Analysis

For analysis of Cvt9 by Optiprep gradients, *cvt9*Δ cells transformed with pCuCVT9(416) were incubated with 50 μM $CuSO_4$ for 1 h to induce Cvt9 expression. At midlog stage the cells were spheroplasted and lysed in gradient buffer (PS200 containing 1 mM $MgCl_2$, 1 mM DTT, 1 mM EDTA, and Complete™ EDTA-free protease inhibitor cocktail). After a preclearing step at 100 *g* at 4°C for 5 min in an Eppendorf 5415D microcentrifuge, the lysate was separated into high-speed supernatant and pellet fractions by direct centrifugation at 100,000 *g* for 20 min at 4°C using a

TLA100.4 rotor. The total membrane fraction was resuspended in gradient buffer and loaded to the top of a 10 ml Optiprep linear gradient (0–66%) and centrifuged in an SW41 rotor at 100,000 *g* for 16 h at 4°C. 14 fractions were collected and analyzed by immunoblotting.

Microscopy

Confocal Microscopy. The *cvt9*Δ cells transformed with pCuGFPCVT9(416) were induced with 10 μM $CuSO_4$ for 2 h, followed by labeling of vacuoles with FM 4-64 and viewing the cells using a confocal microscope (IRM; Leica) as described previously (Kim et al., 1999).

Fluorescence Microscopy. Cells expressing GFP/HA-Gsa9 were grown in glucose or methanol for 2–24 h. FM 4-64 (20 μg/ml) was added and the cells were incubated for an additional 16 h. Cells grown on methanol were transferred to glucose medium for 1–3 h. The cells were then washed and examined immediately using an Axiophot fluorescence microscope (ZEISS). Image capture was done using a SPOT digital camera (Diagnostic Instruments, Inc.) with Adobe Photoshop® software.

Electron Microscopy. Cells were grown for 40 h in medium supplemented with 0.5% methanol and then transferred to medium containing 2% glucose for 2 h. The cells were washed with distilled water and fixed in 1.5% $KMnO_4$. The cells were then dehydrated, embedded in Epon 812, and sectioned for viewing on a JEOL 100CX transmission electron microscope (Yuan et al., 1999).

Coimmunoprecipitation of Cvt9 and Apg1

Cells expressing the NH_2-terminally myc-tagged Cvt9 and HA-tagged Apg1 were grown to midlog phase in YPD and spheroplasted as described previously (Kamada et al., 2000). The spheroplasts were lysed with ice-chilled Tween lysis buffer (50 mM Tris-HCl, pH 7.5, 150 mM NaCl, 1 mM EDTA, 1 mM EGTA, 0.4 mM Na_3VO_4, 50 mM KF, 20 μg/ml leupeptin, 20 μg/ml benzamidine, 10 μg/ml pepstatin A, 40 μg/ml aprotinin, 1 mM PMSF, and 0.5% Tween-20). The lysate was centrifuged at 4,000 *g* for 5 min and precleared with 20 μl of protein G–Sepharose (50% suspension) for 30 min at 4°C. The cell lysate (500 μl) was incubated with or without 3 μl of anti-Apg1 antiserum for 2.5 h at 4°C. Immunocomplexes were collected on protein G–Sepharose beads and washed three times with Tween lysis buffer. The resultant immunocomplexes were subjected to 7.5% SDS-PAGE and analyzed further by immunoblotting with anti-myc ascite (9E10) to detect myc-tagged Cvt9 or with anti-HA ascite (16B12) to detect HA-tagged Apg1. Coimmunoprecipitation of 3×HA-Cvt9 and 3×myc-Cvt9 was performed in essentially the same manner.

Results

The *apg* and *cvt* mutants share a significant genetic overlap, indicating a mechanistic convergence between autophagy and the Cvt pathway (for review see Kim and Klionsky, 2000). Therefore, the strong sensitivity to nitrogen starvation displayed by most autophagy mutants has been used as a phenotypic screen to isolate the complementing plasmids for the majority of the *cvt* and *apg* mutants cloned thus far. Although *cvt9* exhibited only marginal sensitivity to nitrogen starvation, we nevertheless used the starvation screen in an attempt to enrich for *cvt9* cells containing the *CVT9*-complementing plasmid. The *cvt9* mutant was transformed with a yeast genomic library and subjected to nitrogen starvation. After 30 d of this regime, 1 out of the first 100 surviving colonies screened exhibited a reversal of the prAPI accumulation phenotype. The plasmid was isolated and the complementing ORF was determined to be YPR049C, which was named *CVT9*. Further genetic analysis confirmed that *CVT9* mapped to the same locus as the original *cvt9* mutation (see Materials and Methods).

Cvt9 Is Required for Cvt Transport but Not Autophagy

The *CVT9* single-copy plasmid rescued the prAPI processing defect in the *cvt9* mutant strain (Fig. 1 A), although overexpression of Cvt9 using a multicopy *CVT9* plasmid resulted in a moderate accumulation of prAPI. Although the *CVT9* clone was isolated using the nitrogen starvation strategy, the viability of the *cvt9*-null strain remained relatively robust in starvation conditions when compared with a typical mutant in the autophagy pathway (e.g., *cvt10*/*apg1*; Scott et al., 1996; Fig. 1 B). Viability under starvation conditions reflects a capacity for autophagy, indicating an ability to recycle cytosolic material after delivery to the vacuole. Therefore, we next determined if the resistance to nitrogen starvation exhibited by the *cvt9*Δ strain reflects its ability to carry out autophagy.

The proteolytic processing of prAPI to its mature form in the vacuole provides a useful marker to assess the proper function of the Cvt pathway in nutrient-rich conditions and the autophagy pathway under starvation conditions (Scott et al., 1996). In mutants that exhibit both Cvt and autophagy defects (e.g., *apg7*Δ; Kim et al., 1999; Fig. 1 C), prAPI accumulation persists in nutrient-rich as well as starvation conditions. However, if a mutant displays a defect only in Cvt transport (e.g., *cvt3*; Harding et al., 1995; Scott et al., 1996; Fig. 1 C), then the accumulated prAPI phenotype can be rescued by diverting prAPI transport from a defective Cvt pathway to a functional autophagy pathway after shifting cells to starvation conditions. In *cvt9*Δ, the prAPI delivery defect observed in nutrient-rich conditions could be circumvented by a shift to nitrogen starvation conditions, suggesting that a functional autophagy pathway exists to transport prAPI to the vacuole (Fig. 1 C).

To further demonstrate the competence for autophagic uptake in *cvt9*Δ, we examined the recombinant cytosolic marker protein Pho8Δ60. Truncating the NH_2-terminal transmembrane domain in the vacuolar hydrolase (ALP or Pho8) results in its cytosolic localization (Noda et al., 1995). This modified protein is delivered to the vacuole solely by autophagy. Proteolytic cleavage of the Pho8Δ60 propeptide in the vacuole lumen generates the active form of the enzyme, which can be detected by an activity assay (Fig. 1 D) or by immunoblot analysis (data not shown). Wild-type, *apg1*Δ, and *cvt9*Δ strains were transformed with an integrating plasmid that replaced the *PHO8* gene with *pho8*Δ*60*. Cells were vegetatively grown to midlog phase and then shifted to nitrogen starvation conditions to induce autophagy. After 4 h in SD-N, vacuolar ALP activity was measured (Fig. 1 D). The ALP activity in the wild-type strain increased significantly in SD-N, indicating that Pho8Δ60 delivery and subsequent processing to its enzymatically active form occurred in the vacuole. As expected, the shift to SD-N did not increase the ALP activity in the autophagy-defective strain *apg1*Δ. However, in *cvt9*Δ, incubation in nitrogen starvation conditions caused a strong increase in ALP activity, further demonstrating that Cvt9 is not essential for autophagic transport.

The fusion of double membrane Cvt vesicles or autophagosomes with the vacuole releases the single-membrane Cvt or autophagic body into the vacuole lumen, respectively (Baba et al., 1997). The subsequent breakdown of these Cvt or autophagic bodies is dependent on resident hydrolases, as treatment with protease inhibitors such as PMSF will prevent the breakdown of these sin-

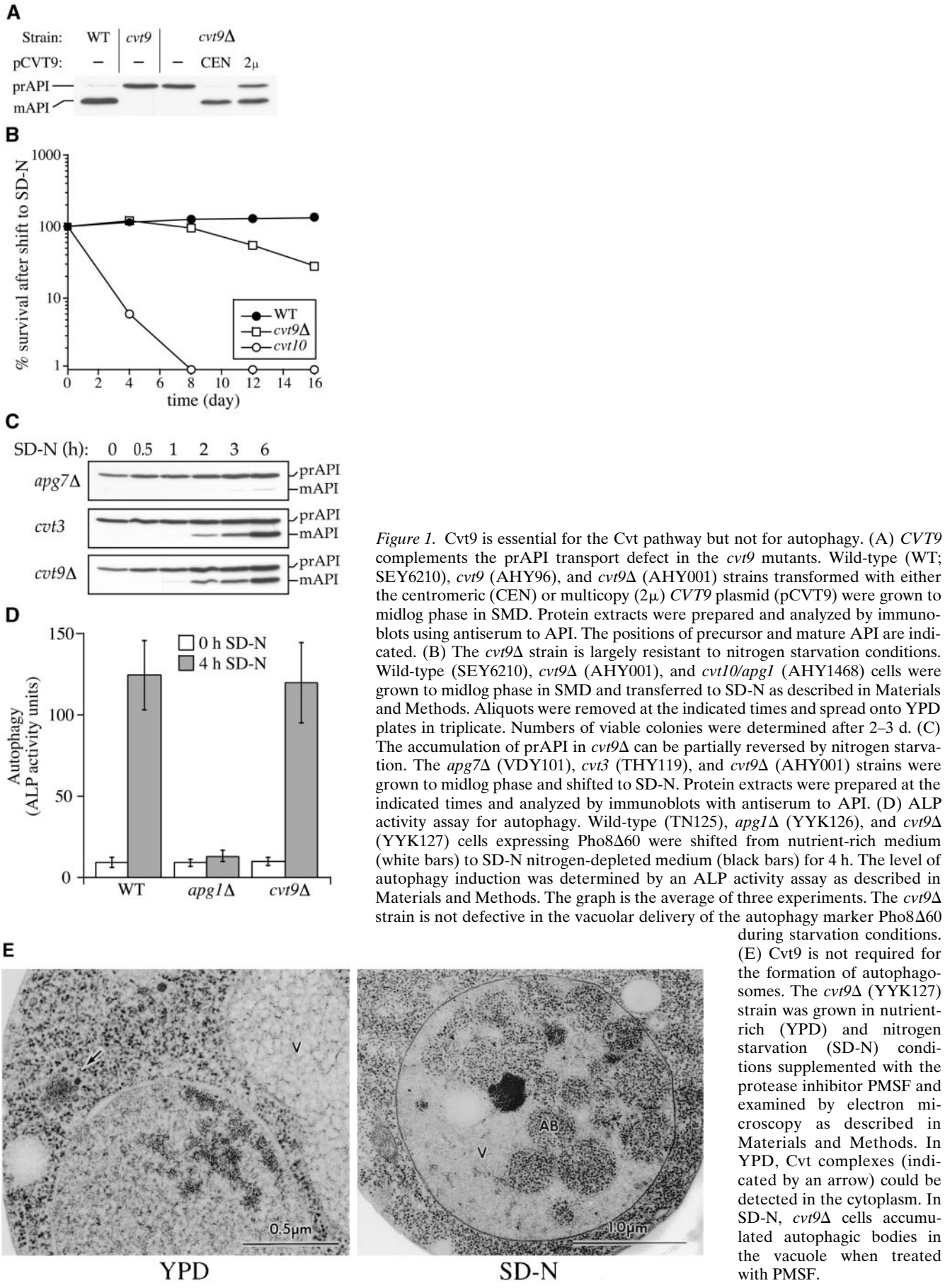

Figure 1. Cvt9 is essential for the Cvt pathway but not for autophagy. (A) *CVT9* complements the prAPI transport defect in the *cvt9* mutants. Wild-type (WT; SEY6210), *cvt9* (AHY96), and *cvt9*Δ (AHY001) strains transformed with either the centromeric (CEN) or multicopy (2μ) *CVT9* plasmid (pCVT9) were grown to midlog phase in SMD. Protein extracts were prepared and analyzed by immunoblots using antiserum to API. The positions of precursor and mature API are indicated. (B) The *cvt9*Δ strain is largely resistant to nitrogen starvation conditions. Wild-type (SEY6210), *cvt9*Δ (AHY001), and *cvt10/apg1* (AHY1468) cells were grown to midlog phase in SMD and transferred to SD-N as described in Materials and Methods. Aliquots were removed at the indicated times and spread onto YPD plates in triplicate. Numbers of viable colonies were determined after 2–3 d. (C) The accumulation of prAPI in *cvt9*Δ can be partially reversed by nitrogen starvation. The *apg7*Δ (VDY101), *cvt3* (THY119), and *cvt9*Δ (AHY001) strains were grown to midlog phase and shifted to SD-N. Protein extracts were prepared at the indicated times and analyzed by immunoblots with antiserum to API. (D) ALP activity assay for autophagy. Wild-type (TN125), *apg1*Δ (YYK126), and *cvt9*Δ (YYK127) cells expressing Pho8Δ60 were shifted from nutrient-rich medium (white bars) to SD-N nitrogen-depleted medium (black bars) for 4 h. The level of autophagy induction was determined by an ALP activity assay as described in Materials and Methods. The graph is the average of three experiments. The *cvt9*Δ strain is not defective in the vacuolar delivery of the autophagy marker Pho8Δ60 during starvation conditions. (E) Cvt9 is not required for the formation of autophagosomes. The *cvt9*Δ (YYK127) strain was grown in nutrient-rich (YPD) and nitrogen starvation (SD-N) conditions supplemented with the protease inhibitor PMSF and examined by electron microscopy as described in Materials and Methods. In YPD, Cvt complexes (indicated by an arrow) could be detected in the cytoplasm. In SD-N, *cvt9*Δ cells accumulated autophagic bodies in the vacuole when treated with PMSF.

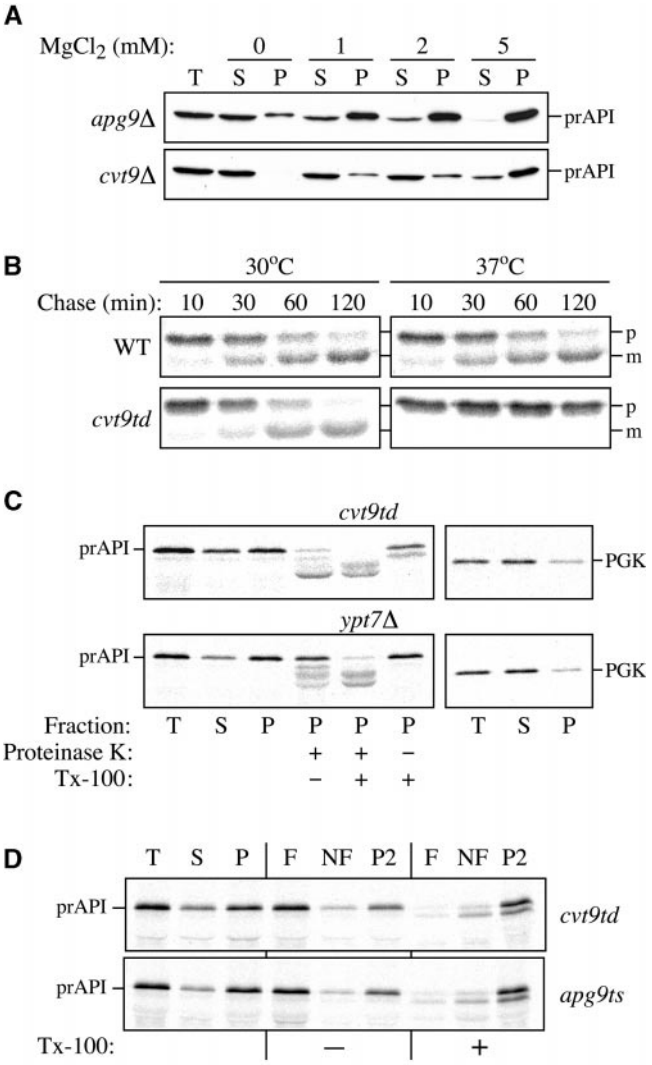

Figure 2. CVT9 mutations destabilize prAPI membrane binding and cause a defect in vesicle formation. (A) prAPI membrane binding is destabilized in the *cvt9*Δ mutant. The *cvt9*Δ (AHY001) and *apg9*Δ (JKY007) strains were grown to midlog phase and converted to spheroplasts. The spheroplasts were lysed in osmotic lysis buffer supplemented with 0, 1, 2, or 5 mM $MgCl_2$. The total lysate (T) was separated into low speed supernatant (S) and pellet (P) fractions by centrifugation at 2,300 *g* for 5 min. The fractionated samples were subjected to immunoblot analysis using antiserum to API. (B) The temperature-conditional *cvt9td* strain is tightly blocked for prAPI import at nonpermissive temperature. Wild-type (WT; SEY6210) and *cvt9td* (JGY9td) strains were incubated at 30°C and 37°C for 5 min, pulse-labeled for 10 min, and then subjected to nonradioactive chase reactions for the indicated times. Samples at each time point were immunoprecipitated with antiserum to API as described in Materials and Methods. (C) prAPI in the *cvt9td* strain is protease accessible. Spheroplasts isolated from *cvt9td* and *ypt7*Δ cells were pulse-labeled for 10 min and chased for 30 min at 37°C. The labeled spheroplasts were then osmotically lysed and separated into low-speed supernatant (S) and pellet (P) fractions after a 2,300-*g* centrifugation step. The pellet fractions were subjected to protease treatment in the absence or presence of 0.2% Triton X-100 as described in Materials and Methods. (D) prAPI in the *cvt9td* strain associates with a floatable membrane fraction. Spheroplasts of *apg9ts* and *cvt9td* were osmotically lysed and separated into supernatant (S) and pellet (P) fractions by centrifugation at 2,300 *g* for 5 min. An aliquot was removed for the total lysate control (T). The pellet fraction (P) was resuspended in 15% Ficoll-400 and added to the bottom of a step gradient of 13 and 2% Ficoll-400. The step gradients were centrifuged at 16,000 *g* for 10 min. Membrane-containing float (F), nonfloat (NF), and pellet (P2) fractions were immunoprecipitated with antiserum to API as described in Materials and Methods.

gle-membrane vesicles inside the vacuole (Takeshige et al., 1992). To obtain morphological evidence for a functional autophagy pathway in the *cvt9*Δ strain, cells were grown in either nutrient-rich or nitrogen starvation conditions in the presence of PMSF and analyzed by electron microscopy (Fig. 1 E). In nutrient-rich conditions when cells were treated with PMSF, Cvt bodies did not accumulate in the vacuole. Instead, Cvt complexes could be occasionally detected in the cytosol, confirming that the Cvt pathway is defective in the *cvt9*-null strain. In contrast, PMSF treatment of *cvt9*Δ cells in nitrogen starvation medium caused a substantial accumulation of autophagic bodies inside the vacuole. Taken together, these findings demonstrate that Cvt9 is required for the Cvt pathway, but does not appear to function in autophagic transport.

The Stability of prAPI Membrane Binding Is Compromised in cvt9Δ

The delivery of prAPI via the Cvt pathway involves the assembly of prAPI oligomers into a Cvt complex that binds a pelletable membrane fraction in a salt-dependent manner (Kim et al., 1997). Subcellular fractionation experiments indicate that prAPI can be recovered entirely in a low-speed pellet fraction in an osmotic lysis buffer containing 5 mM $MgCl_2$, whereas omitting $MgCl_2$ from the lysis buffer results in a completely cytosolic distribution of prAPI (Oda et al., 1996). Furthermore, in vitro reconstitution experiments in buffer containing 5 mM $MgCl_2$ demonstrate that membrane-bound prAPI can subsequently be transported into the vacuole, suggesting that the salt-dependent membrane binding of prAPI represents a bona fide step in the transport pathway and not a byproduct of protein aggregation (Scott et al., 1996). We next examined the function of Cvt9 in the context of the stability of prAPI binding to the membrane fraction. The *cvt9*Δ cells were grown to midlog phase and converted into spheroplasts. The spheroplasts were lysed in an osmotic lysis buffer in the presence of titrating concentrations of $MgCl_2$. The lysates were then separated into low-speed supernatant and pellet fractions and analyzed by immunoblots using antiserum to API as described in Materials and Methods. The *apg9*Δ strain was used as a control in which prAPI displays typical membrane-binding properties. In the absence of salt, prAPI association with the pellet fraction is severely perturbed (Fig. 2 A), consistent with previous reports (Oda et al., 1996). In a typical *cvt/apg* mutant such as *apg9*Δ, addition of increasing concentrations of $MgCl_2$ stabilizes the binding of prAPI to the membrane fraction; substantial prAPI binding occurred at 1 mM $MgCl_2$ and nearly complete prAPI association with the pellet fraction was detected in 5 mM $MgCl_2$. In contrast, in the *cvt9*Δ strain,

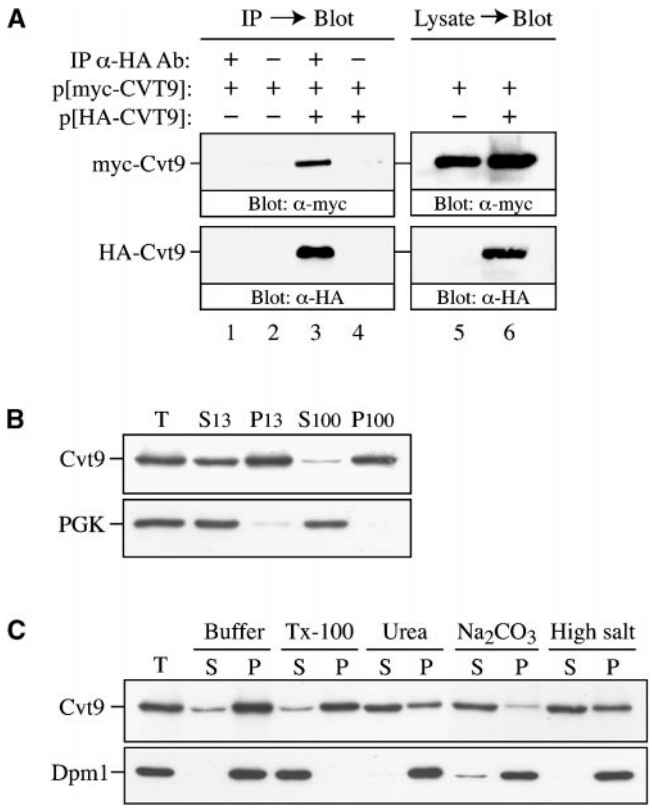

Figure 3. Characterization of Cvt9. (A) Cvt9 forms a homodimer. The wild-type (KA311A) strain was transformed with a plasmid encoding myc-tagged Cvt9 with or without a second plasmid for HA-tagged Cvt9. Cell lysates were prepared as described in Materials and Methods and immunoprecipitated (IP) with antiserum to HA (lanes 1 and 3) or buffer control (lanes 2 and 4). The immunoprecipitates were then immunoblotted with antiserum or antibodies to HA and myc. The anti-HA–precipitated immunocomplex also contains myc-tagged Cvt9. The cell lysates were also directly immunoblotted with anti-HA and anti-myc antibodies to assess the expression of the epitope tagged Cvt9 fusions (lanes 5 and 6). (B) Cvt9 subcellular fractionation pattern. The *cvt9*Δ (AHY001) strain was transformed with a *CVT9* plasmid behind the *CUP1* copper-inducible promoter (pCuCVT9[416]). Expression was induced with 50 μM $CuSO_4$ for 1 h before spheroplasting. The spheroplasts were osmotically lysed (see Materials and Methods). After a preclearing centrifugation step at 100 *g* for 5 min to remove unlysed spheroplasts, the total lysate (T) was separated into low speed supernatant (S13) and pellet (P13) fractions. The S13 fraction was further separated into 100,000 *g* supernatant (S100) and pellet (P100) fractions. The fractionated samples were subjected to immunoblot analysis using antiserum to Cvt9 and the cytosolic marker protein PGK. (C) Cvt9 is a peripheral membrane protein that is detergent resistant. A total lysate was prepared as in B and resuspended in osmotic lysis buffer only or containing 1% Triton X-100, 6 M urea, 0.1 M Na_2CO_3, pH 10.5, or a 1.0 M salt wash (0.67 M KOAc, 0.3 M KCl). The treated lysates were separated into total membrane (P) and supernatant (S) fractions by centrifugation at 100,000 *g* for 20 min at 4°C. The samples were analyzed by immunoblots with antiserum to Cvt9 and antibodies to the ER integral membrane protein Dpm1.

prAPI remained largely in the supernatant fraction even at 2 mM $MgCl_2$, with significant prAPI membrane binding occurring only at 5 mM $MgCl_2$. These results indicate that although Cvt9 is not essential for prAPI membrane binding, the deletion of *CVT9* destabilizes the interactions between prAPI oligomers and the membrane structure to which they bind.

Cvt9 Is Required at the Stage of Cvt Vesicle Formation/Completion

The permanent loss of function in the *cvt9*Δ mutant may result in indirect, secondary phenotypes on the Cvt pathway. To determine the direct effects of Cvt9 loss of function, we generated a temperature-sensitive form of Cvt9 by constructing a chimera of Cvt9 linked to the COOH terminus of Ub-DHFR, resulting in the Cvt9td fusion protein (Dohmen et al., 1994). The expression of Cvt9td was placed under the copper-inducible *CUP1* promoter. At permissive temperature (30°C), the strain (JGY9td) expressing the Cvt9td protein was fully functional for the Cvt pathway and displayed prAPI maturation kinetics that were similar to the wild-type strain (Fig. 2 B). A shift to nonpermissive temperature caused the rapid misfolding and degradation of Cvt9td by proteasome-mediated proteolysis (data not shown; Dohmen et al., 1994). As a consequence, prAPI import was tightly blocked in the *cvt9td* mutant at the nonpermissive temperature, whereas prAPI maturation kinetics remained unaffected in the wild-type strain (Fig. 2 B). The immediate defect in prAPI processing caused by the thermal inactivation of Cvt9td suggests that Cvt9 acts directly in the Cvt pathway.

To determine the step of the pathway in which Cvt9 function is required, we analyzed the state of prAPI in the *cvt9td* strain by protease sensitivity and membrane flotation assays. Cvt9td expression was induced at midlog phase for 1 h with 1 μM $CuSO_4$ before spheroplasting. The *cvt9td* spheroplasts were radioactively labeled for 5 min followed by a nonradioactive chase reaction for 30 min at nonpermissive temperature. The labeled spheroplasts were then lysed osmotically and separated into low-speed supernatant and pellet fractions as described in Materials and Methods. The prAPI-containing pellet fractions were treated with exogenous proteinase K in the presence or absence of detergent and then immunoprecipitated with API antiserum. The supernatant and pellet fractions were also immunoprecipitated with antiserum to the cytosolic marker protein PGK to assess the osmotic spheroplast lysis efficiency. The protease sensitivity assay indicates that at nonpermissive temperature, prAPI in the *cvt9td* strain was accessible to exogenous proteases even in the absence of detergent treatment (Fig. 2 C). The small amount of protease-resistant prAPI in the *cvt9td* strain probably reflects incomplete spheroplast lysis based on the appearance of a small amount of PGK in the pellet fraction. Nevertheless, the protease-protection assay of *cvt9td* at nonpermissive temperature suggests that Cvt vesicles had not yet formed to enclose prAPI in this strain. The *ypt7*Δ mutant was used as the control strain. Ypt7 is a rab guanosine triphosphatase required for Cvt vesicle fusion with the vacuole, and thus the *ypt7*Δ strain accumulates prAPI in a protease-protected state (Fig. 2 C; Kim et al., 1999).

In the membrane flotation gradient analysis, membrane-associated proteins in a cell lysate migrate to the top of a step gradient and are collected as the "float" (F) fraction. Soluble proteins remain in the nonfloat (NF) fraction and proteins associated with large protein complexes are recovered in the gradient pellet fraction (P2). The radiola-

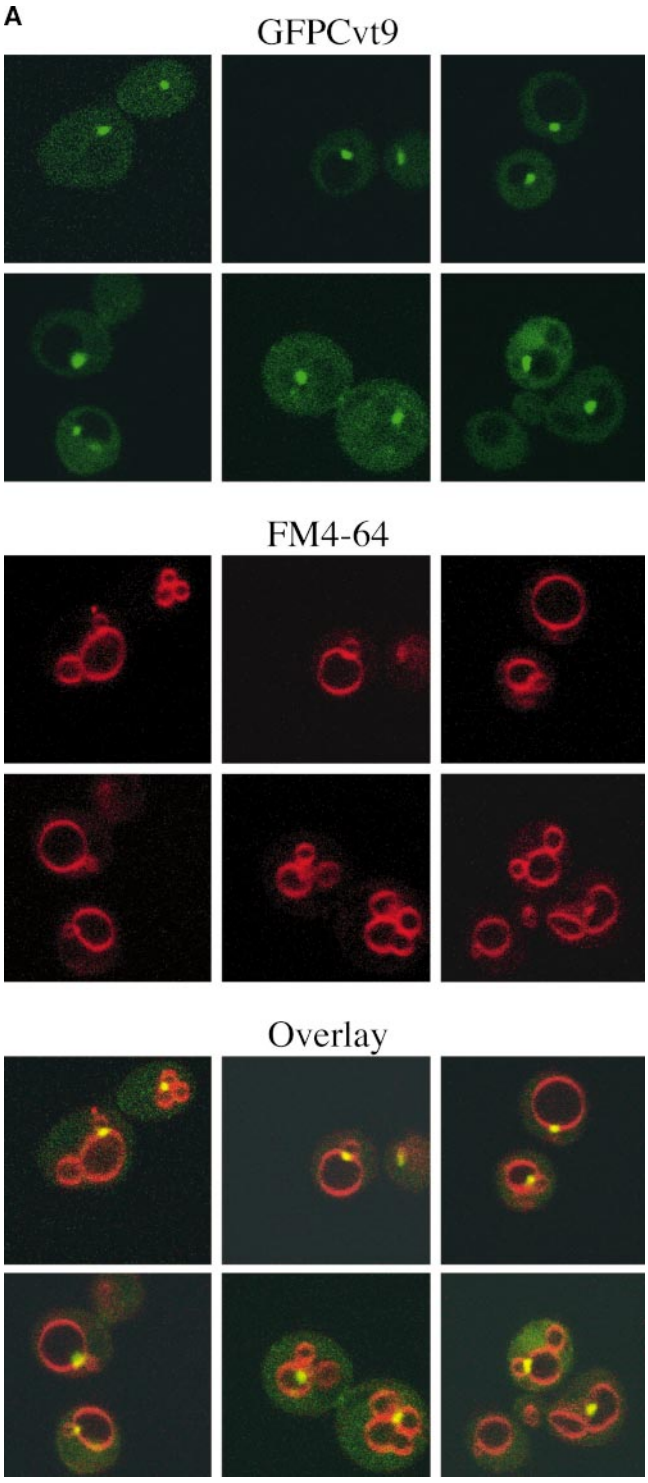

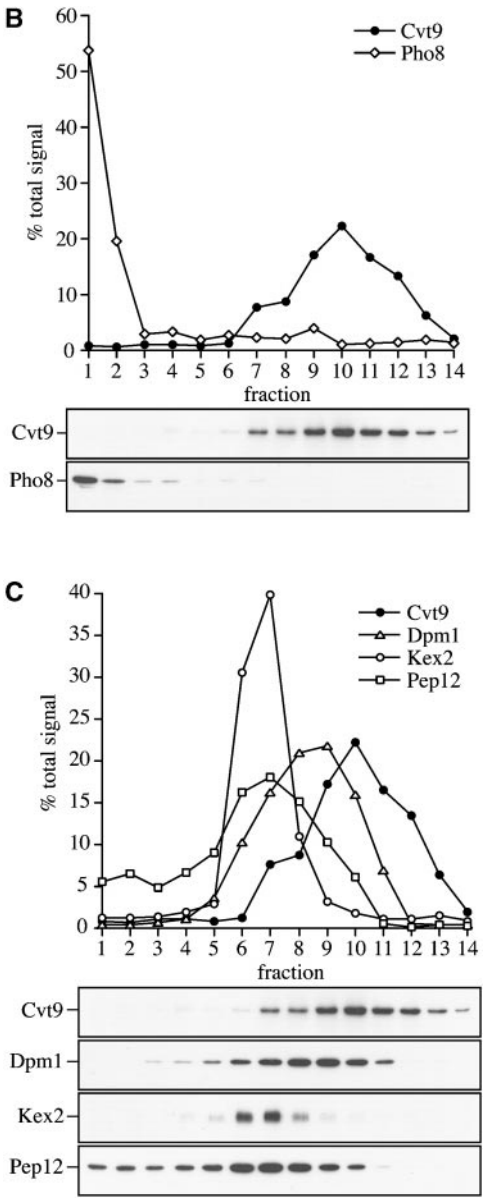

Figure 4. Cvt9 is localized to a perivacuolar compartment. (A) Localization pattern of GFPCvt9. The *cvt9*Δ (AHY001) strain was transformed with a plasmid encoding a GFPCvt9 fusion protein behind the *CUP1* promoter (pCuGFPCVT9). Expression of GFPCvt9 was induced with 10 μM $CuSO_4$ for 2 h, followed by labeling of the vacuoles with FM 4-64 (see Materials and Methods). Images were taken with a Leica IRM confocal microscope. GFPCvt9 mostly localizes to intense perivacuolar, punctate structures. (B and C) Subcellular localization of Cvt9 by Optiprep density gradients. The *cvt9*Δ strain was transformed with pCuCVT9(416) and incubated with 50 μM $CuSO_4$ at midlog growth stage to induce Cvt9 expression. The cells were converted to spheroplasts and lysed in gradient lysis buffer (see Materials and Methods). A total membrane fraction was isolated by centrifugation at 100,000 *g* for 20 min and loaded to the top of a 10-ml Optiprep linear gradient (0–66%). After centrifugation at 100,000 *g* for 16 h at 4°C, 14 fractions were collected and analyzed by immunoblots with antiserum or antibodies to Cvt9 and (B) Pho8 (vacuole), (C) Dpm1 (ER), Kex2 (trans-Golgi Network), and Pep12 (endosome). The immunoblots and the graphs of the densitometry quantitation are from the same gradient but presented separately for clarity.

beled prAPI pellet fraction derived from the lysate of the *cvt9td* strain at nonpermissive temperature was loaded on the bottom of a step gradient and subjected to centrifugation. The majority of prAPI from the *cvt9td* strain was recovered in the float fraction, indicating that prAPI associates with a floatable membrane source (Fig. 2 D). As a positive control for the flotation gradient analysis, we examined the prAPI pellet fraction derived from a temperature-conditional allele of *apg9* (*apg9ts*). Consistent with our recent study on Apg9, prAPI from the *apg9ts* strain as-

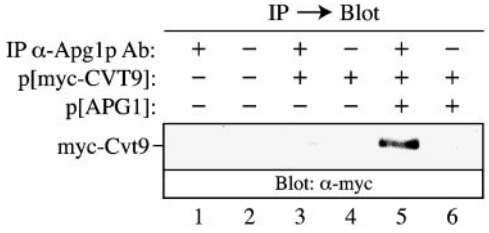

Figure 5. Cvt9 physically associates with Apg1. The *apg1*Δ strain (YYK36) was transformed with a plasmid encoding myc-tagged Cvt9 (p[myc-CVT9]) with or without an additional plasmid encoding Apg1 (p[APG1]). The cell lysates were prepared as described in Materials and Methods and subjected to immunoprecipitation with anti-Apg1 antiserum (lanes 1, 3, and 5) or buffer only (lanes 2, 4, and 6). The immunoprecipitates (IP) were analyzed by immunoblot with antiserum to myc. The anti-Apg1–precipitated immunocomplex contains myc-tagged Cvt9 (lane 5).

sociates with a membrane source and is recovered in the float fraction (Noda et al., 2000). Taken together, these findings demonstrate that Cvt9 is directly required for the completion of Cvt vesicles and appears to stabilize the association of prAPI with these forming vesicles.

Cvt9 Is an Oligomeric, Coiled Coil, Peripheral Membrane Protein

To further understand Cvt9 function in the Cvt pathway, we next characterized the biosynthesis of the Cvt9 protein. Polyclonal antiserum raised against synthetic Cvt9 peptides recognized a 135-kD band by immunoblot analysis, in agreement with its predicted molecular mass (data not shown). Detection of Cvt9 increased in *cvt9*Δ cells transformed with the *CVT9* multicopy plasmid and was absent in the *cvt9*Δ cells, suggesting that the antiserum is specific for the Cvt9 protein. Analysis of the Cvt9 amino acid sequence reveals a significant coiled coil secondary structure between amino acid residues 542 and 851 (http://nightingale.lcs.mit.edu/cgi-bin/score). The *P. pastoris* homologue, Gsa9, also contains a predicted coiled coil secondary structure motif between amino acids 811 and 1027. Because a common feature of proteins containing a coiled coil domain is the ability to form higher-ordered quaternary structures, we investigated the possibility that Cvt9 forms oligomers. Extracts from cells expressing NH_2-terminally myc-tagged Cvt9 and HA-tagged Cvt9 were prepared and the immunocomplex containing HA-Cvt9 was immunoprecipitated under native, nonreducing conditions with antiserum to the HA epitope. A subsequent anti-myc epitope immunoblot detected the myc-tagged Cvt9 from the original immunoprecipitated HA–Cvt9 immunocomplex, indicating that myc-Cvt9 associates with HA–Cvt9 (Fig. 3 A). These findings indicate that Cvt9 forms homodimers or potentially larger oligomeric structures.

The subcellular location of Cvt9 was initially examined by subcellular fractionation and differential centrifugation procedures. The *cvt9*Δ strain was transformed with a plasmid containing *CVT9* behind the *CUP1* copper regulable promoter (Labbé and Thiele, 1999). Cvt9 expression was induced at midlog phase with 50 μM $CuSO_4$ for 1 h before spheroplasting. The prAPI accumulation in the *cvt9*Δ strain was completely reversed at this level of Cvt9 expression (data not shown). The spheroplasts were lysed osmotically and separated into low-speed supernatant and pellet fractions (S13 and P13, respectively). The S13 supernatant fraction was further resolved into high-speed supernatant and pellet fractions (S100 and P100, respectively). The majority of Cvt9 fractionated to both the P13 and P100 fractions, whereas only a minor population appeared in the high-speed supernatant fraction (Fig. 3 B). We next investigated the nature of the Cvt9 pellet association (Fig. 3 C). The spheroplasts were lysed osmotically and treated with lysis buffer, Triton X-100, urea, Na_2CO_3, or a high salt wash as described in Materials and Methods. The treated lysates were then subjected to high-speed centrifugation and separated into total membrane and supernatant fractions. The buffer-only treatment confirmed that the majority of Cvt9 remained bound to a membrane pellet fraction. However, treatment with urea, Na_2CO_3, and the high-salt wash, conditions that remove peripheral membrane proteins, all stripped a substantial portion of Cvt9 from the membrane pellet into the supernatant fraction. In addition, examination of Cvt9 by membrane flotation gradient analysis indicated that Cvt9 was recovered in the "float" fraction, suggesting that it associated with a floatable membrane (data not shown). Therefore, we propose that Cvt9 is a peripheral membrane protein (Fig. 3 C). In contrast, the integral membrane protein Dpm1 remained in the pellet fraction under all conditions, except when membranes were solubilized with detergent. Interestingly, Cvt9 remained in the pellet fraction after treatment with Triton X-100, suggesting that Cvt9 multimers may form a larger detergent-resistant protein complex.

Cvt9 Localizes to a Distinct Perivacuolar Compartment

To investigate the identity of the membrane compartment with which Cvt9 associates, a GFP fusion to the NH_2 terminus of Cvt9 was examined. Under the control of the *CUP1* promoter, GFPCvt9 expression complemented the prAPI defect in the *cvt9*Δ strain, indicating that it was a functional chimera (data not shown). At midlog stage, *cvt9*Δ cells expressing GFPCvt9 were labeled with FM 4-64 to mark the vacuoles and examined by confocal microscopy. GFPCvt9 appeared to be concentrated at prominent punctate structures directly adjacent to FM 4-64–labeled vacuoles (Fig. 4 A). A weak, cytosolic distribution of GFPCvt9 was also detected, consistent with the ratio of Cvt9 found in the membrane pellet and cytosolic supernatant fractions by biochemical fractionation analysis (compare Figs. 3 B and 4 A).

The confocal micrographs of GFPCvt9 suggested residence in a compartment proximal to the vacuole or directly on the vacuolar membrane in the form of a concentrated patch. To identify the Cvt9 compartment relative to known membrane marker proteins, we next examined Cvt9 subcellular localization by linear Optiprep density gradients (Fig. 4, B and C). Expression of Cvt9 was induced with 50 μM $CuSO_4$ for 1 h before spheroplasting. A total membrane fraction was prepared from osmotically lysed spheroplasts and resolved on Optiprep gradients as described in Materials and Methods. Immunoblot analysis of the collected gradient fractions indicated a peak for the Pho8-localized vacuole compartment in fraction 1, whereas the Cvt9 compartment migrated to a much denser region, with a peak in fraction 10 (Fig. 4 B). This finding demonstrates that the perivacuolar Cvt9 compartment is

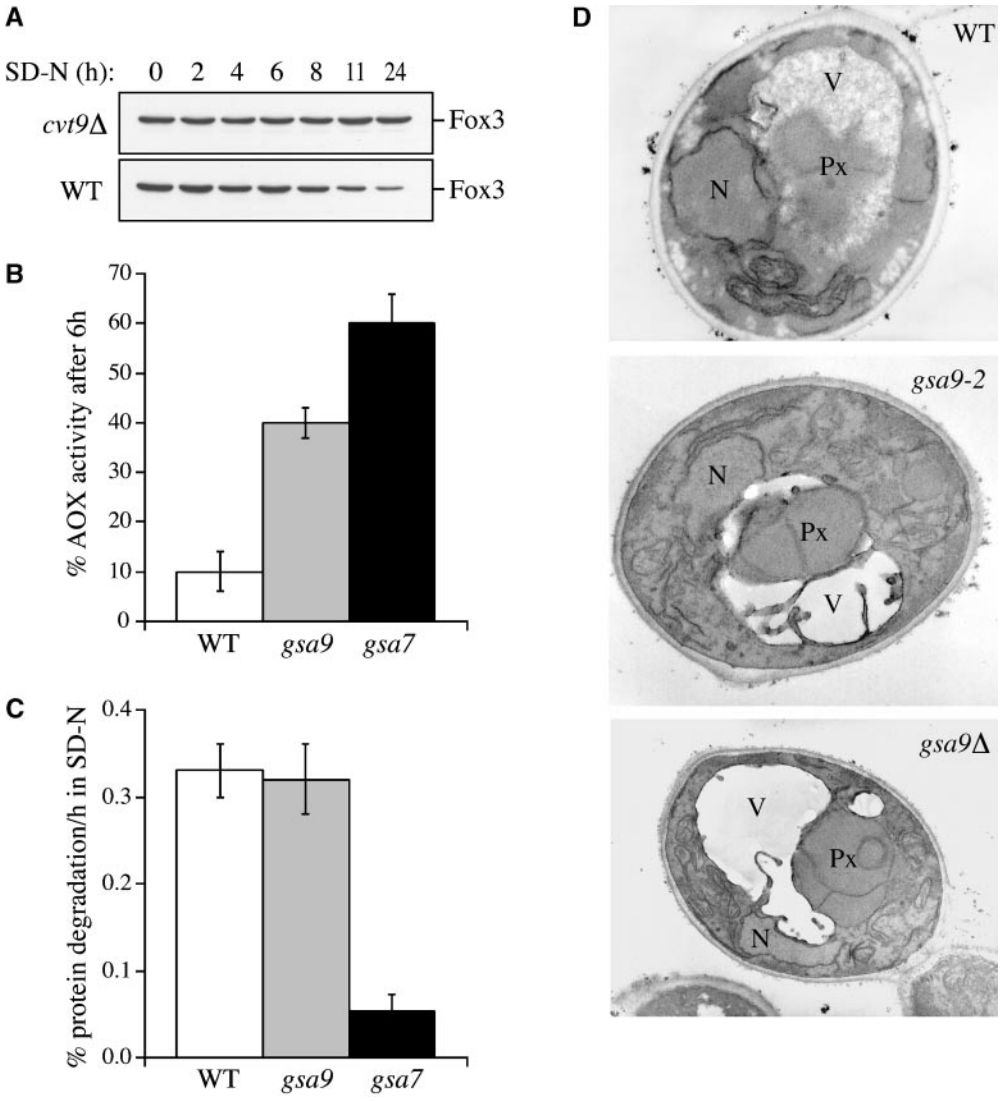

Figure 6. Cvt9 and the *P. pastoris* homologue Gsa9 are required for peroxisome degradation. (A) The *S. cerevisiae cvt9*Δ strain is defective in pexophagy. Peroxisomes from wild-type (WT; KA311A) and *cvt9*Δ (YYK107) cells were proliferated in oleic acid medium and then degraded by shifting to SD-N medium at the indicated times (see Materials and Methods). Pexophagy was monitored by immunoblot analysis of the peroxisomal thiolase enzyme, Fox3. Fox3 levels decrease in wild-type cells under pexophagy conditions but remain constant in *cvt9*Δ. (B) The *P. pastoris gsa9* strain is defective in pexophagy. Peroxisomes from wild-type (GS115), *gsa7* (WDY7), and *gsa9* (R8) cells were proliferated in methanol medium and then degraded by shifting to glucose medium for 0 and 6 h (see Materials and Methods). Pexophagy was measured by an activity assay for the peroxisomal AOX enzyme. AOX activity decreases in wild-type cells in glucose adaptation conditions, but remains relatively high in *gsa7* and *gsa9* cells. (C) The *P. pastoris gsa9*Δ strain is not defective in autophagy. Wild-type (GS115), *gsa7* (WDY7), and *gsa9* (R8) cells were radiolabeled with 1 μCi/ml [^{14}C]valine for 16 h. The cells were then shifted to nitrogen-depleted chase medium and the production of TCA-soluble radioactivity was measured during 2–24 h of chase. Protein turnover rate in *gsa9* cells is comparable to wild-type cells but relatively low in the autophagy-defective *gsa7* cells. (D) The *P. pastoris gsa9* mutants are defective at a middle to late stage of micropexophagy. Wild-type strain (GS115) and mutant strains *gsa9-2* (R8) and *gsa9Δ* (WDK09) were grown to confluency under methanol conditions to proliferate peroxisomes. The strains were then shifted to a glucose-containing medium for 2 h to induce peroxisome degradation before fixation and processing for electron microscopy (see Materials and Methods). Partially degraded peroxisomes (Px) were found within the vacuole (V) of the parental GS115 cells. This was not observed in the *gsa9-2* and *gsa9Δ* mutants. Instead, arm-like extensions of the vacuole(s) were observed to partially surround the peroxisomes. The nuclei (N) are also indicated.

distinct from the vacuole. Furthermore, the Cvt9 compartment did not appear to cofractionate with any other resident organelle marker proteins, including Dpm1 (ER), Kex2 (late Golgi apparatus), and Pep12 (endosome) (Fig. 4 C). Taken together, the identity of the perivacuolar compartment to which Cvt9 localizes appears to be distinct from known organelles of the endomembrane system.

Cvt9 Physically Interacts with the Apg1 Kinase

Cvt9 is present in a detergent-resistant form, presumably a protein complex, which localizes to a distinct membrane compartment (Figs. 3 and 4). We next identified an additional factor of the Cvt9 protein complex. A two-hybrid analysis to identify proteins that associate with the autophagy component Apg1 identified Cvt9 as a potential interacting partner (Kamada et al., 2000). The Apg1–Cvt9 interaction was directly supported by a coimmunoprecipitation analysis (Fig. 5). The *apg1*Δ strain was transformed with the plasmid encoding the myc-tagged Cvt9 fusion protein with or without a second plasmid encoding Apg1. Cell extracts were immunoprecipitated with antiserum to Apg1 under native, nondenaturing conditions as described in Materials and Methods. The precipitated immunocomplexes were then subjected to a denaturing SDS-PAGE/immunoblot procedure with antiserum to the myc epitope. In cells expressing both myc–Cvt9 and Apg1, the immunocomplexes precipitated with the Apg1 antiserum also isolated the myc-tagged Cvt9 protein, thus confirming the two-hybrid data that Apg1 and Cvt9 physically interact (Fig. 5, lane 5).

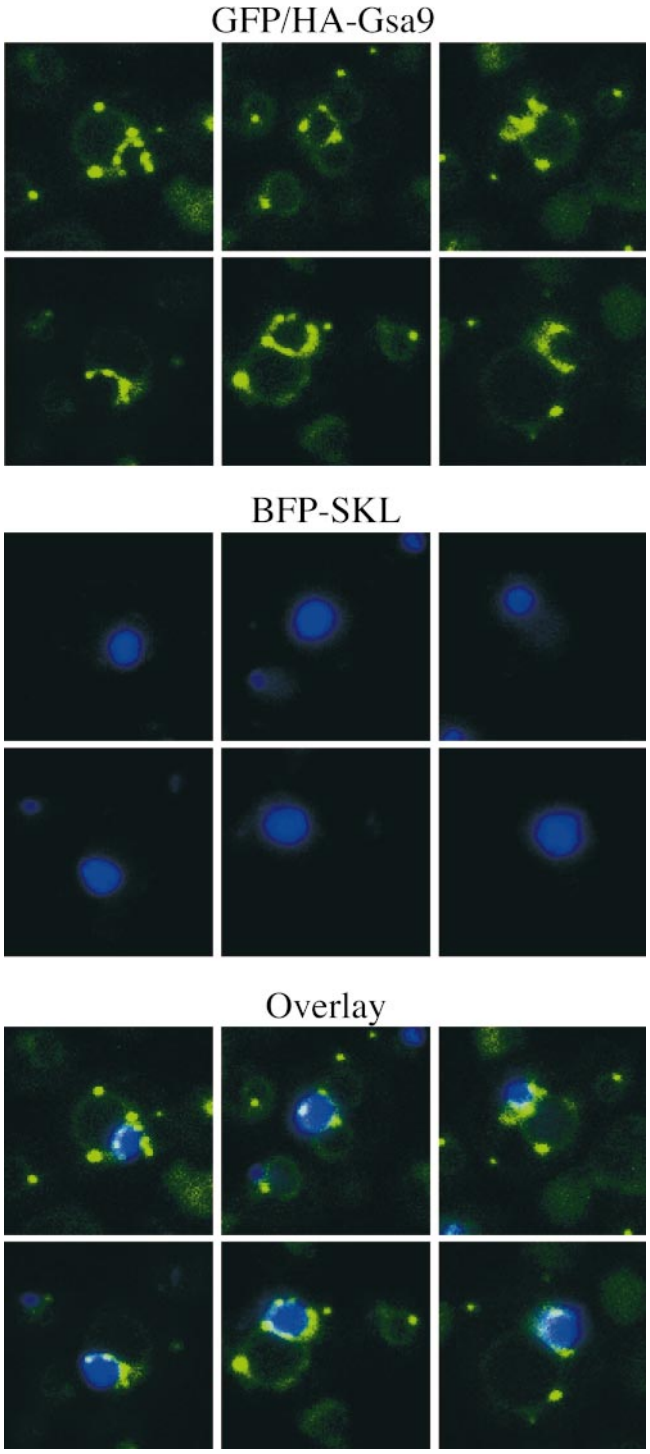

Figure 7. GFP/HA-Gsa9 localization during glucose adaptation. ANB23 cells expressing both BFP fused at its COOH terminus to the serine-lysine-leucine (SKL) peroxisomal targeting signal (BFP-SKL) and GFP/HA-Gsa9 were grown under methanol conditions, then adapted to glucose for 4 h. The peroxisomes were labeled by BFP-SKL (middle). During glucose adaptation, the GFP/HA-Gsa9 (top) was concentrated to regions of the vacuolar membrane that engulf the peroxisomes containing the BFP-SKL marker (see overlay in bottom panels). A punctate GFP/HA-Gsa9 pattern was also detected.

Cvt9 and Its P. pastoris Homologue, Gsa9, Are both Required for Peroxisome Degradation

We identified *GSA9* as an essential component for the glucose-stimulated peroxisome degradation pathway in *P. pastoris*. Sequence analysis revealed *GSA9* to be a structural and functional homologue of *CVT9*. Both proteins contain a predicted coiled coil domain. However, although many proteins encoded by the *S. cerevisiae* genome share common residues in the coiled coil domain, only Cvt9 shows extensive homology with its *P. pastoris* counterpart over the entire sequence. More specifically, a BLAST search with the NH_2-terminal and COOH-terminal Gsa9 domains (amino acids 1–810 and 1028–1316, respectively) flanking its predicted coiled coil region was performed against all *S. cerevisiae* proteins (http://genome-www2.stanford.edu/cgi-bin/SGD/nph-blast2sgd). The BLAST results identified the corresponding NH_2-terminal and COOH-terminal domains flanking the coiled coil region of Cvt9 as the only sequences with statistically significant similarity to Gsa9 (*P* value, 3.9×10^{-19} and 3.9×10^{-17}, respectively). This sequence analysis indicates that Cvt9 is the sole homologue of Gsa9 in *S. cerevisiae* and does not represent one member in a family of related proteins.

To determine if Cvt9 was also required for the specific degradation of peroxisomes in *S. cerevisiae*, we examined the degradation of Fox3, the peroxisomal thiolase enzyme, following a previously described method for examining pexophagy in *S. cerevisiae* (Hutchins et al., 1999). Peroxisome proliferation was induced in *cvt9*Δ and wild-type cells by growth in oleic acid medium. Upon shift to SD-N medium to induce pexophagy, peroxisome degradation was examined by monitoring cellular Fox3 levels over the indicated time course (Fig. 6 A). In wild-type cells, Fox3 levels decreased significantly over the time course, whereas they remained constant in *cvt9*Δ cells. This finding suggests that Cvt9 is required for the specific, vacuolar delivery of not only prAPI via the Cvt pathway, but also peroxisomes via the pexophagy pathway in *S. cerevisiae*.

The *P. pastoris gsa9* mutant was further characterized to better understand the cellular function of Gsa9. Peroxisomes and the expression of resident enzymes, such as AOX, were induced in methanol-containing medium. The peroxisomes were then degraded upon shift to glucose-containing medium. After a 6-h incubation in glucose adaptation conditions, AOX activity was measured (Fig. 6 B). Wild-type GS115 cells displayed significant loss of AOX activity, indicating that excess peroxisomes were degraded via pexophagy. As a negative control, *gsa7* cells were analyzed. *GSA7* is the *P. pastoris* homologue of *APG7*, an essential component for pexophagy as well as the Cvt pathway and autophagy (Yuan et al., 1999). Both *gsa7* and *gsa9* cells retained substantial AOX activity upon glucose adaptation, confirming the roles of these proteins in peroxisome degradation.

As we have noted, Cvt9 does not play an integral role in starvation-induced autophagy (Fig. 1). If Gsa9 functions in an analogous manner, then *gsa9* mutants should also be competent for autophagic degradation. Autophagy accounts for the majority of the cellular degradative capacity during starvation conditions (for review see Kim and Klionsky, 2000). Thus, the degree of autophagy can be

measured in terms of total protein turnover under nitrogen starvation conditions. Wild-type, *gsa7*, and *gsa9* cells were labeled with [^{14}C]valine, followed by a nonradioactive chase reaction in nitrogen starvation medium. The production of TCA-soluble radioactivity was measured over the course of 2–24 h. The autophagy-defective *gsa7* strain exhibited a low rate of protein turnover, whereas the relative protein degradation rate in *gsa9* cells appeared similar to the wild-type, suggesting that *gsa9* is not defective in autophagy (Fig. 6 C).

The process of micropexophagy can be categorized into distinct stages (Sakai et al., 1998). During the early steps of glucose adaptation, peroxisomes associate with the vacuolar membrane. Arm-like extensions of the vacuole initiate the peroxisome engulfment process. In the middle stage(s), vacuolar extensions become more pronounced, ultimately surrounding the peroxisomes. This is followed by the late stage(s), which involves a homotypic fusion event to fully enclose the peroxisomes inside the vacuole. Subsequent breakdown of the peroxisome-containing inner vacuolar vesicle triggers the eventual degradation of the peroxisomes. To determine the stage at which Gsa9 is required during micropexophagy, we examined wild-type, *gsa9-2*, and *gsa9*Δ strains by electron microscopy (Fig. 6 D). In wild-type cells, peroxisomes could be occasionally detected undergoing degradation in the vacuolar lumen. However, both *gsa9-2* and *gsa9*Δ cells exhibited a micropexophagy defect at a middle/late stage in which vacuolar extensions only partially surround the peroxisome but do not complete the engulfment process.

Gsa9 Is Recruited to the Vacuolar Membrane during Peroxisome Uptake

To further characterize the role of Gsa9 in micropexophagy, we examined its localization by fluorescence microscopy using a functional GFP/HA-Gsa9 fusion protein. This construct was able to complement the *gsa9Δ* phenotype (data not shown). In cells that have not been subjected to glucose adaptation conditions, GFP/HA-Gsa9 appeared localized to one or two structures adjacent to the vacuole (data not shown). In addition, a weak GFP/HA-Gsa9 signal was detected coincident with the FM 4-64–labeled vacuoles. The punctate pattern of GFP/HA-Gsa9 appeared nearly identical to the localization pattern of GFPCvt9, although we could not detect GFPCvt9 on the vacuole (Fig. 4 A). When cells expressing GFP/HA-Gsa9 were grown in methanol medium to proliferate peroxisomes and then subjected to adaptation in glucose medium, the GFP/HA-Gsa9 signal localized predominantly to the vacuolar membrane (Fig. 7, top). To compare GFP/HA-Gsa9 localization to that of peroxisomes, we constructed a blue fluorescent protein (BFP) tagged with the serine-lysine-leucine COOH-terminal peroxisomal targeting signal (BFP-SKL; Fig. 7, middle). In glucose adaptation conditions, the intensity of GFP/HA-Gsa9 appeared strongest at the vacuolar regions that surrounded the peroxisomes during the engulfment process (Fig. 7, bottom). GFP/HA-Gsa9 also formed punctate structures that appeared continuous with its vacuolar membrane labeling pattern. The distribution of GFP/HA-Gsa9 before and after glucose adaptation suggests that Gsa9 localizes to regions of the vacuolar membrane that contact peroxisomes during micropexophagy.

Discussion

Autophagy and the Cvt pathway are overlapping processes that share most components. However, the Cvt pathway operates in a biosynthetic capacity during vegetative conditions, whereas autophagy is primarily a degradative process that is induced by starvation. Both pathways involve dynamic membrane rearrangements to deliver cytosolic contents to the vacuole. Morphological studies suggest that the two pathways normally operate exclusively of one another. The regulatory mechanisms and structural differences that control the conversion between the Cvt pathway and autophagy are not well understood. To gain further insight into the factors that are distinct between these pathways, we have examined a protein component, Cvt9, and its *P. pastoris* homologue, Gsa9, which appear to be specific to the Cvt pathway and micropexophagy, respectively.

Cvt9 Forms a Protein Complex Comprised of Cvt/Apg Phosphoproteins

Cvt9 exists primarily as a peripherally bound membrane protein (Fig. 3, B and C). Coimmunoprecipitation results demonstrate that it forms homodimers or even higher order homooligomers (Fig. 3 A), potentially through a coiled coil assembly mechanism, as indicated by secondary structural analysis. Consistent with our recent two-hybrid results (Kamada et al., 2000), we have demonstrated by coimmunoprecipitation analysis that Cvt9 directly interacts with the serine/threonine kinase Apg1 (Fig. 5), a component essential for both Cvt transport and autophagy. The association with Apg1 places Cvt9 as a member of a larger putative protein complex comprised of other components of the Cvt and autophagy pathways including Apg1, Apg13, Apg17, and Vac8 (Kamada et al., 2000; Scott et al., 2000). However, it remains to be determined if these Cvt/Apg components assemble into one protein complex or whether they represent separate, discrete interactions. Recent studies have demonstrated stable physical interactions between Apg1 and Apg13, Apg1 and Apg17, and Vac8 and Apg13 (Kamada et al., 2000; Scott et al., 2000). Apg13, together with Apg1, represent the components in the putative protein complex that are required for both Cvt transport and autophagy (Scott et al., 1996, 2000). In contrast, Apg17 is required for autophagy but not the Cvt pathway (Kamada et al., 2000), whereas Vac8 does not appear to be essential for autophagy but is required for the Cvt pathway (Scott et al., 2000). Similar to the *vac8* phenotype, the *cvt9* mutant also displays the hallmarks of a functional autophagy pathway, including viability under nutrient deprivation, the ability to transport bulk cytosol to the vacuole, and the accumulation of autophagic bodies when vesicle breakdown is pharmacologically inhibited (Fig. 1).

The differential effects that Cvt9, Apg1, Apg13, Apg17, and Vac8 exert on the Cvt and autophagy pathways suggest that these components may serve to regulate the conversion between Cvt transport and autophagy. Apg1,

Apg13, Cvt9, and Vac8 are all phosphoproteins, and the phosphorylation state and affinity of Apg13 to Apg1 are regulated by nutrient conditions through the Tor kinase cascade (Matsuura et al., 1997; Kamada et al., 2000; Scott et al., 2000). Taken together, these findings suggest that these regulatory proteins may serve as a junction at which upstream signals based on nutrient availability are transduced to effect the downstream formation of either Cvt vesicles or autophagosomes.

The Cvt9 Protein Complex Localizes to a Novel Perivacuolar Compartment

The subcellular distribution of GFPCvt9 supports an increasingly familiar localization pattern among Cvt and autophagy components (Kim et al., 1999; Noda et al., 2000). Specifically, an intense concentration of the GFPCvt9 fusion protein appears at a punctate, perivacuolar structure (Fig. 4 A). This localization pattern corresponds to a subcellular density profile distinct from other known membrane compartments, including ER, Golgi, and the Pep12-localized endosome (Fig. 4 B and C). Given that Cvt9 associates with Apg1, which in turn interacts with additional components essential for autophagy, the Cvt pathway, and pexophagy, the putative Cvt9 protein complex may identify, at the molecular level, a novel membrane compartment critical for these modes of subcellular trafficking.

Mechanistic Similarities between the Cvt/Autophagy Pathways and Micropexophagy

In *P. pastoris*, the specific degradation of excess peroxisomes during glucose adaptation entails the sequestration of peroxisomes by the vacuole in the process of micropexophagy. The mechanistic details of how a Cvt vesicle or an autophagosome forms to sequester cargo appear morphologically similar to the vacuole-mediated engulfment of peroxisomes. In each case, the sequestration of cargo by a membrane source results in the formation of a double-membrane structure. In the case of micropexophagy, the enwrapping membrane is the vacuole itself whereas the membrane source in the formation of Cvt vesicles and autophagosomes remains to be determined.

We have identified Gsa9 as the *P. pastoris* homologue of Cvt9. The functional analysis of Gsa9 corroborates and may provide new insights into the role of Cvt9 in *S. cerevisiae*. Neither Gsa9 nor Cvt9 is required for autophagy, whereas both are essential for peroxisome degradation (Figs. 1 and 6). The degradation of peroxisomes in *S. cerevisiae* may occur by micropexophagy (Chiang et al., 1996). In *P. pastoris*, the uptake of peroxisomes by micropexophagy is easily detected and thus the morphological consequence of a *gsa9* mutation can be readily assessed. Electron micrographs reveal that the arrest in micropexophagy occurs at a middle sequestration stage in the *gsa9* mutant. That is, the vacuole(s) only partially surrounds the peroxisomes but cannot complete the engulfment process (Fig. 6 D).

The prAPI phenotype in *cvt9* supports a similar defect in the Cvt pathway. To characterize the direct effect of Cvt9 inactivation, we constructed a Cvt9 temperature-degron fusion protein (Cvt9td), a novel temperature-conditional form of Cvt9 (Fig. 2 B). At nonpermissive temperature, prAPI in the *cvt9td* strain remained protease accessible (Fig. 2 C). In addition, prAPI was able to float through a step gradient in a detergent-dependent manner, suggesting that it associated with a floatable membrane (Fig. 2 D). Therefore, the *cvt9* defect in the Cvt pathway may be at a middle-to-late stage in Cvt vesicle formation, analogous to the *gsa9* mutant phenotype for micropexophagy.

Localization of Gsa9 Versus Cvt9

A key difference between Gsa9 and Cvt9 is their subcellular localization patterns. Before the induction of micropexophagy, Gsa9 appears to be localized to both a punctate structure in the perivacuolar region and diffusely distributed on the vacuole (data not shown). However, upon glucose adaptation, a population of Gsa9 strongly localizes to regions of the vacuolar membrane that are in contact with peroxisomes in the process of being sequestered into the vacuole (Fig. 7). In contrast, the localization of Cvt9 to the perivacuolar compartment appears constant regardless of nutrient status. If Cvt9 functions analogously to Gsa9 in the Cvt pathway of *S. cerevisiae*, then it may directly participate in the enwrapping of prAPI-containing Cvt complexes to form the double-membrane Cvt vesicles. Furthermore, if Cvt9 acts at the site of cargo sequestration in an analogous manner to the function of Gsa9 at the vacuole during peroxisome engulfment, then the Cvt9 localization pattern would identify the perivacuolar compartment as the donor membrane source for Cvt vesicles. Additional studies will be required to test this assertion.

Potential Function of Gsa9 and Cvt9

Given that the mechanisms of the Cvt pathway and pexophagy are quite similar to autophagy (for review see Kim and Klionsky, 2000), why is autophagy not affected in the *cvt9* and *gsa9* mutants? The function of Cvt9 and Gsa9 may be required for the recognition of specific cargo, such as prAPI and peroxisomes, but not for the sequestration of nonspecific bulk cytosol by autophagy. The observation that Gsa9 appears to be concentrated in a region of the vacuolar membrane that contacts the peroxisome during the engulfment process suggests that Gsa9 may function in the recognition of peroxisomes. Without Gsa9, the proper associations between the peroxisomal and vacuolar membranes may not exist, resulting in a checkpoint stop in the engulfment process. The role of Gsa9 and Cvt9 as potential factors that provide cargo specificity is supported by the observation that deleting Cvt9 destabilizes the binding of prAPI-containing Cvt complexes to the membrane (Fig. 2 A). In addition, the role of Cvt9 in prAPI specificity can also be examined in terms of the prAPI reversal phenotype. Under nitrogen starvation conditions, prAPI accumulation is only partially reversed in the *cvt9*Δ strain (Fig. 1 C). If a deletion in *CVT9* did not affect the selective nature of prAPI import, then one would predict that the entire population of prAPI would enter the vacuole via autophagy. The near complete reversal of prAPI under starvation conditions is observed in some API propeptide mutants that retain the ability to bind to the membrane (Scott et al., 1997). In contrast, the import of the bulk cytosolic marker Pho8Δ60 via autophagy plateaus at ~30%. Therefore, the loss of cargo selectivity in the *cvt9*Δ strain may result in the recognition of prAPI as another nonspe-

cific molecule during autophagy. Further analysis of Cvt9 and the proteins that associate with it will provide additional information about the conversion between the Cvt pathway and autophagy as well as the mechanism that modulates specificity in the Cvt pathway and pexophagy.

We thank Maria Hutchins for advice and helpful discussions on pexophagy; Kimberley Eggerton, Andrew Bevan, and Denny Player for technical assistance; and Wei-Pang Huang, Chao-Wen Wang, and Drs. Sarah Teter and Hagai Abeliovich for critical reading of the manuscript. We also thank Dr. Jürgen Dohmen for supplying the plasmids used in constructing the *cvt9td* mutant and Dr. Dennis Thiele for supplying the vectors containing the yeast *CUP1* inducible copper promoter.

This work was supported by Public Health Service grant GM53396 from the National Institutes of Health to D.J. Klionsky, Grants-in-Aid for Scientific Research from the Ministry of Education, Science, and Culture of Japan to Y. Ohsumi, a grant from The Norwegian Cancer Society to P.E. Stromhaug, and National Science Foundation grant MCB-9817002 to W.A. Dunn, Jr.

Submitted: 23 October 2000
Revised: 30 January 2001
Accepted: 20 February 2001

References

Baba, M., K. Takeshige, N. Baba, and Y. Ohsumi. 1994. Ultrastructural analysis of the autophagic process in yeast: detection of autophagosomes and their characterization. *J. Cell Biol.* 124:903–913.

Baba, M., M. Osumi, and Y. Ohsumi. 1995. Analysis of the membrane structures involved in autophagy in yeast by freeze-replica method. *Cell Struct. Funct.* 20:465–471.

Baba, M., M. Osumi, S.V. Scott, D.J. Klionsky, and Y. Ohsumi. 1997. Two distinct pathways for targeting proteins from the cytoplasm to the vacuole/lysosome. *J. Cell Biol.* 139:1687–1695.

Baum, P., J. Thorner, and L. Honig. 1978. Identification of tubulin from the yeast *Saccharomyces cerevisiae*. *Proc. Natl. Acad. Sci. USA*. 75:4962–4966.

Becherer, K.A., S.E. Rieder, S.D. Emr, and E.W. Jones. 1996. Novel syntaxin homologue, Pep12p, required for the sorting of lumenal hydrolases to the lysosome-like vacuole in yeast. *Mol. Biol. Cell*. 7:579–594.

Chiang, H.L., R. Schekman, and S. Hamamoto. 1996. Selective uptake of cytosolic, peroxisomal, and plasma membrane proteins into the yeast lysosome for degradation. *J. Biol. Chem.* 271:9934–9941.

Cregg, J.M., K.J. Barringer, A.Y. Hessler, and K.R. Madden. 1985. *Pichia pastoris* as a host system for transformations. *Mol. Cell. Biol.* 5:3376–3385.

Darsow, T., S.E. Rieder, and S.D. Emr. 1997. A multispecificity syntaxin homologue, Vam3p, essential for autophagic and biosynthetic protein transport to the vacuole. *J. Cell Biol.* 138:517–529.

Dohmen, R.J., P. Wu, and A. Varshavsky. 1994. Heat-inducible degron: a method for constructing temperature-sensitive mutants. *Science*. 263:1273–1276.

George, M.D., M. Baba, S.V. Scott, N. Mizushima, B.S. Garrison, Y. Ohsumi, and D.J. Klionsky. 2000. Apg5p functions in the sequestration step in the cytoplasm-to-vacuole targeting and macroautophagy pathways. *Mol. Biol. Cell*. 11:969–982.

Gerhardt, B., T.J. Kordas, C.M. Thompson, P. Patel, and T. Vida. 1998. The vesicle transport protein Vps33p is an ATP-binding protein that localizes to the cytosol in an energy-dependent manner. *J. Biol. Chem.* 273:15818–15829.

Harding, T.M., K.A. Morano, S.V. Scott, and D.J. Klionsky. 1995. Isolation and characterization of yeast mutants in the cytoplasm to vacuole protein targeting pathway. *J. Cell Biol.* 131:591–602.

Harding, T.M., A. Hefner-Gravink, M. Thumm, and D.J. Klionsky. 1996. Genetic and phenotypic overlap between autophagy and the cytoplasm to vacuole protein targeting pathway. *J. Biol. Chem.* 271:17621–17624.

Hutchins, M.U., M. Veenhuis, and D.J. Klionsky. 1999. Peroxisome degradation in *Saccharomyces cerevisiae* is dependent on machinery of macroautophagy and the Cvt pathway. *J. Cell Sci.* 112:4079–4087.

Irie, K., M. Takase, K.S. Lee, D.E. Levin, H. Araki, K. Matsumoto, and Y. Oshima. 1993. *MKK1* and *MKK2*, which encode *Saccharomyces cerevisiae* mitogen-activated protein kinase-kinase homologs, function in the pathway mediated by protein kinase C. *Mol. Cell. Biol.* 13:3076–3083.

Kamada, Y., T. Funakoshi, T. Shintani, K. Nagano, M. Ohsumi, and Y. Ohsumi. 2000. Tor-mediated induction of autophagy via an Apg1 protein kinase complex. *J. Cell Biol.* 150:1507–1513.

Kametaka, S., A. Matsuura, Y. Wada, and Y. Ohsumi. 1996. Structural and functional analyses of *APG5*, a gene involved in autophagy in yeast. *Gene*. 178:139–143.

Kim, J., and D.J. Klionsky. 2000. Autophagy, cytoplasm-to-vacuole targeting pathway, and pexophagy in yeast and mammalian cells. *Annu. Rev. Biochem.* 69:303–342.

Kim, J., S.V. Scott, M. Oda, and D.J. Klionsky. 1997. Transport of a large oligomeric protein by the cytoplasm to vacuole protein targeting pathway. *J. Cell Biol.* 137:609–618.

Kim, J., V.M. Dalton, K.P. Eggerton, S.V. Scott, and D.J. Klionsky. 1999. Apg7p/Cvt2p is required for the cytoplasm-to-vacuole targeting, macroautophagy, and peroxisome degradation pathways. *Mol. Biol. Cell*. 10:1337–1351.

Kim, J., S.V. Scott, and D.J. Klionsky. 2000. Alternative protein sorting pathways. *Int. Rev. Cytol.* 198:153–201.

Klionsky, D.J., and S.D. Emr. 2000. Autophagy as a regulated pathway of cellular degradation. *Science*. 290:1717–1721.

Klionsky, D.J., and Y. Ohsumi. 1999. Vacuolar import of proteins and organelles from the cytoplasm. *Annu. Rev. Cell. Dev. Biol.* 15:1–32.

Klionsky, D.J., R. Cueva, and D.S. Yaver. 1992. Aminopeptidase I of *Saccharomyces cerevisiae* is localized to the vacuole independent of the secretory pathway. *J. Cell Biol.* 119:287–299.

Labbé, S., and D.J. Thiele. 1999. Copper ion inducible and repressible promoter systems in yeast. *Methods Enzymol.* 306:145–153.

Liang, X.H., S. Jackson, M. Seaman, K. Brown, B. Kempkes, H. Hibshoosh, and B. Levine. 1999. Induction of autophagy and inhibition of tumorigenesis by *beclin 1*. *Nature*. 402:672–676.

Matsuura, A., M. Tsukada, Y. Wada, and Y. Ohsumi. 1997. Apg1p, a novel protein kinase required for the autophagic process in *Saccharomyces cerevisiae*. *Gene*. 192:245–250.

Mizushima, N., T. Noda, T. Yoshimori, Y. Tanaka, T. Ishii, M.D. George, D.J. Klionsky, M. Ohsumi, and Y. Ohsumi. 1998. A protein conjugation system essential for autophagy. *Nature*. 395:395–398.

Mizushima, N., T. Noda, and Y. Ohsumi. 1999. Apg16p is required for the function of the Apg12p-Apg5p conjugate in the yeast autophagy pathway. *EMBO (Eur. Mol. Biol. Organ.) J.* 18:3888–3896.

Mortimore, G.E., G. Miotto, R. Venerando, and M. Kadowaki. 1996. Autophagy. *Subcell. Biochem.* 27:93–135.

Nakamura, N., A. Matsuura, Y. Wada, and Y. Ohsumi. 1997. Acidification of vacuole is required for the autophagic degradation in the yeast *Saccharomyces cerevisiae*. *J. Biochem.* 121:338–344.

Noda, T., and Y. Ohsumi. 1998. Tor, a phosphatidylinositol kinase homologue, controls autophagy in yeast. *J. Biol. Chem.* 273:3963–3966.

Noda, T., A. Matsuura, Y. Wada, and Y. Ohsumi. 1995. Novel system for monitoring autophagy in the yeast *Saccharomyces cerevisiae*. *Biochem. Biophys. Res. Commun.* 210:126–132.

Noda, T., J. Kim, W.-P. Huang, M. Baba, C. Tokunaga, Y. Ohsumi, and D.J. Klionsky. 2000. Apg9p/Cvt7p is an integral membrane protein required for transport vesicle formation in the Cvt and autophagy pathways. *J. Cell Biol.* 148:465–480.

Oda, M.N., S.V. Scott, A. Hefner-Gravink, A.D. Caffarelli, and D.J. Klionsky. 1996. Identification of a cytoplasm to vacuole targeting determinant in aminopeptidase 1. *J. Cell Biol.* 132:999–1010.

Rieder, S.E., and S.D. Emr. 1997. A novel RING finger protein complex essential for a late step in protein transport to the yeast vacuole. *Mol. Biol. Cell*. 8:2307–2327.

Robinson, J.S., D.J. Klionsky, L.M. Banta, and S.D. Emr. 1988. Protein sorting in *Saccharomyces cerevisiae*: isolation of mutants defective in the delivery and processing of multiple vacuolar hydrolases. *Mol. Cell. Biol.* 8:4936–4948.

Rose, M.D., P. Novick, J.H. Thomas, D. Botstein, and G.R. Fink. 1987. A *Saccharomyces cerevisiae* genomic plasmid bank based on a centromere-containing shuttle vector. *Gene*. 60:237–243.

Sakai, Y., A. Koller, L.K. Rangell, G.A. Keller, and S. Subramani. 1998. Peroxisome degradation by microautophagy in *Pichia pastoris*: identification of specific steps and morphological intermediates. *J. Cell Biol.* 141:625–636.

Sato, T.K., T. Darsow, and S.D. Emr. 1998. Vam7p, a SNAP-25-like molecule, and Vam3p, a syntaxin homolog, function together in yeast vacuolar protein trafficking. *Mol. Cell. Biol.* 18:5308–5319.

Sato, T.K., P. Rehling, M.R. Peterson, and S.D. Emr. 2000. Class C Vps protein complex regulates vacuolar SNARE pairing and is required for vesicle docking/fusion. *Mol. Cell*. 6:661–671.

Scott, S.V., A. Hefner-Gravink, K.A. Morano, T. Noda, Y. Ohsumi, and D.J. Klionsky. 1996. Cytoplasm to vacuole targeting and autophagy employ the same machinery to deliver proteins to the yeast vacuole. *Proc. Natl. Acad. Sci. USA*. 93:12304–12308.

Scott, S.V., M. Baba, Y. Ohsumi, and D.J. Klionsky. 1997. Aminopeptidase I is targeted to the vacuole by a nonclassical vesicular mechanism. *J. Cell Biol.* 138:37–44.

Scott, S.V., D.C. Nice III, J.J. Nau, L.S. Weisman, Y. Kamada, I. Keizer-Gunnink, T. Funakoshi, M. Veenhuis, Y. Ohsumi, and D.J. Klionsky. 2000. Apg13p and Vac8p are part of a complex of phosphoproteins that are required for cytoplasm to vacuole targeting. *J. Biol. Chem.* 275:25840–25849.

Seals, D.F., G. Eitzen, N. Margolis, W.T. Wickner, and A. Price. 2000. A Ypt/Rab effector complex containing the Sec1 homolog Vps33p is required for homotypic vacuole fusion. *Proc. Natl. Acad. Sci. USA*. 97:9402–9407.

Sears, I.B., J. O'Connor, O.W. Rossanese, and B.S. Glick. 1998. A versatile set of vectors for constitutive and regulated gene expression in *Pichia pastoris*. *Yeast*. 14:783–790.

Shintani, T., N. Mizushima, Y. Ogawa, A. Matsuura, T. Noda, and Y. Ohsumi. 1999. Apg10p, a novel protein-conjugating enzyme essential for autophagy

in yeast. *EMBO (Eur. Mol. Biol. Organ.) J.* 18:5234–5241.
Takeshige, K., M. Baba, S. Tsuboi, T. Noda, and Y. Ohsumi. 1992. Autophagy in yeast demonstrated with proteinase-deficient mutants and conditions for its induction. *J. Cell Biol.* 119:301–311.
Tanida, I., N. Mizushima, M. Kiyooka, M. Ohsumi, T. Ueno, Y. Ohsumi, and E. Kominami. 1999. Apg7p/Cvt2p: a novel protein-activating enzyme essential for autophagy. *Mol. Biol. Cell.* 10:1367–1379.
Teter, S.A., K.P. Eggerton, S.V. Scott, J. Kim, A.M. Fischer, and D.J. Klionsky. 2001. Degradation of lipid vesicles in the yeast vacuole requires function of Cvt17, a putative lipase. *J. Biol. Chem.* 276:2083–2087.
Thumm, M., R. Egner, M. Koch, M. Schlumpberger, M. Straub, M. Veenhuis, and D.H. Wolf. 1994. Isolation of autophagocytosis mutants of *Saccharomyces cerevisiae*. *FEBS Lett.* 349:275–280.
Tsukada, M., and Y. Ohsumi. 1993. Isolation and characterization of autophagy-defective mutants of *Saccharomyces cerevisiae*. *FEBS Lett.* 333:169–174.
Tuttle, D.L., and W.A. Dunn, Jr. 1995. Divergent modes of autophagy in the methylotrophic yeast *Pichia pastoris*. *J. Cell Sci.* 108:25–35.
Vittorini, S., C. Paradiso, A. Donati, G. Cavallini, M. Masini, Z. Gori, M. Pollera, and E. Bergamini. 1999. The age-related accumulation of protein carbonyl in rat liver correlates with the age-related decline in liver proteolytic activities. *J. Gerontol. A Biol. Sci. Med. Sci.* 54:B318–B323.
Wurmser, A.E., and S.D. Emr. 1998. Phosphoinositide signaling and turnover: PtdIns(3)P, a regulator of membrane traffic, is transported to the vacuole and degraded by a process that requires lumenal vacuolar hydrolase activities. *EMBO (Eur. Mol. Biol. Organ.) J.* 17:4930–4942.
Yuan, W., D.L. Tuttle, Y.J. Shi, G.S. Ralph, and W.A. Dunn, Jr. 1997. Glucose-induced microautophagy in *Pichia pastoris* requires the α-subunit of phosphofructokinase. *J. Cell Sci.* 110:1935–1945.
Yuan, W., P.E. Stromhaug, and W.A. Dunn, Jr. 1999. Glucose-induced autophagy of peroxisomes in *Pichia pastoris* requires a unique E1-like protein. *Mol. Biol. Cell.* 10:1353–1366.